eLIFE elifesciences.org

RESEARCH ARTICLE

Figures and figure supplements

Visual projection neurons in the *Drosophila* lobula link feature detection to distinct behavioral programs

Ming Wu *et al*

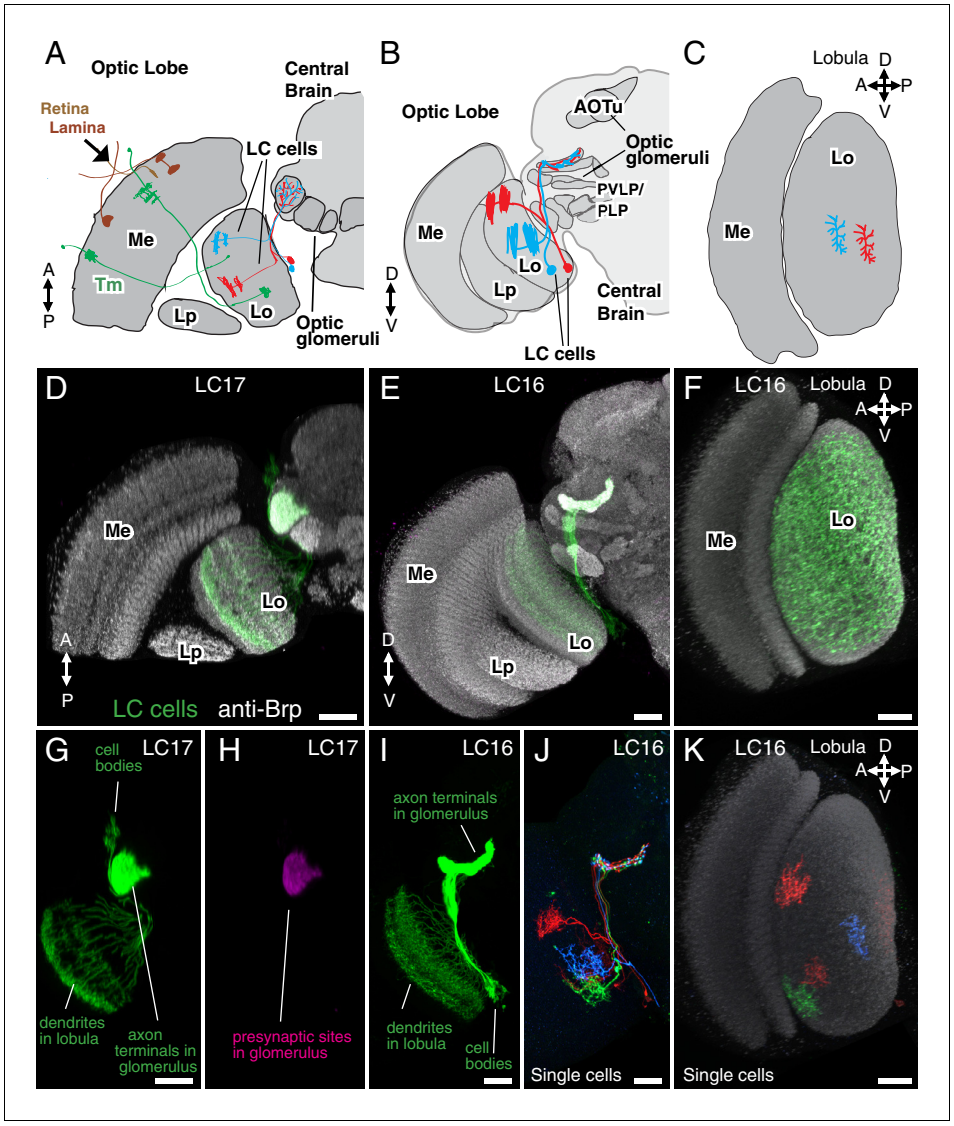

Figure 1. Introduction to lobula columnar (LC) neurons. Schematics (**A–C**) and confocal images (**D–K**) show the lobula and adjacent parts of the visual system. (**A,D,G,H**) Horizontal sections. (**B,E,I,J**) Anterior views. (**C,F,K**) Cross-section views of the lobula. Some subregions of the optic lobe (Me, Medulla; Lp, Lobula plate; Lo, Lobula) and central brain (AOTu, Anterior Optic Tubercle; PVLP, Posterior Ventrolateral Protocerebrum; PLP, Posterior Lateral Protocerebrum) are indicated in selected panels. Dendrites of individual LC neurons (red and blue cells in the schematics and red, blue and green cells in J,K) span only part of the visual field. As populations, the neurons of a given LC cell type cover most or all of the lobula (**F**), though LC neurons with regionally restricted lobula arbors also exist (e.g. LC14 (***Otsuna and Ito, 2006***), see ***Figure 1—figure supplement 1***). LC neurons receive feed forward visual inputs from photoreceptors in the retina via a series of optic lobe interneurons (a few lamina neurons, in brown, and transmedullary neurons [Tm], in green, are illustrated as examples in [A]). This places LC neurons at least 2–3 synapses downstream of the photoreceptors. The majority of LC neurons projects to distinct target regions in the central brain called optic glomeruli; some of these are illustrated in (**A**) and (**B**) and also visible as distinct structures in the anti-Brp pattern in the images in (**D**) and (**E**). Most optic glomeruli are located in the PVLP and the adjacent more posterior PLP. The more dorsal AOTu (illustrated in [**B**]) is considered a specialized optic glomerulus. For a more detailed map of optic glomeruli see ***Figure 3***. Confocal images show either populations of neurons (**D–I**) or individual cells labeled using Multicolor FlpOut (MCFO) (***Nern et al., 2015***) (**J,K**). LC cell types shown are LC17 (**D,G,H**) and LC16 (**E,F,I–K**). Population labeling (**D–I**) was with split-GAL4 driven expression of a membrane marker (green; myr::smFLAG, using pJFRC225-5XUAS-IVS-myr::smFLAG in *VK00005*) with a presynaptic marker also shown [magenta; synaptotagmin-HA, using pJFRC51-3XUAS-IVS-syt::smHA in *su(Hw)attP1*] in (**D,E**) and by itself in (**H**). A neuropil marker (anti-Brp) is included in grey in (**D–F,K**) and

Figure 1 continued on next page

Figure 1 continued

neuropil regions are also in grey in the schematics. Images in (**D,E,G–J**) were generated using brains that were computationally aligned to a template brain using the anti-Brp pattern as reference. The anti-Brp pattern in (**D,E**) is that of the standard brain used for alignment. Images in (**D–K**) show projection images of different views of three-dimensional image stacks; these were generated in either Fiji (http://fiji.sc/) (**D,E,G–J**) or Vaa3D (***Peng et al., 2010***) (**F,K**). Scale bars represent 20 μm.

DOI: 10.7554/eLife.21022.003

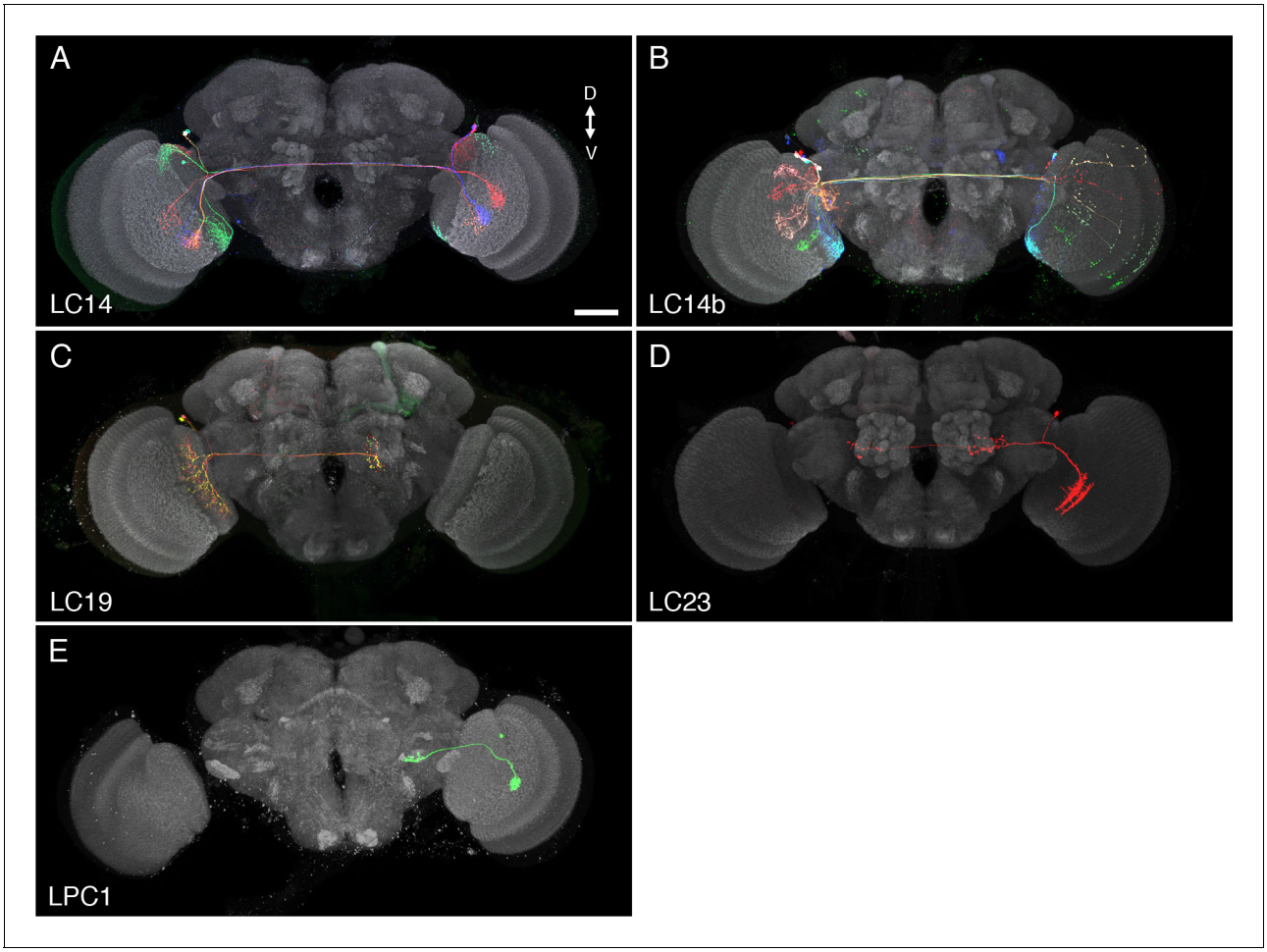

Figure 1—figure supplement 1. Examples of additional LC cell types and similar neurons. These cell types were not selected for further analyses in this study since they did not project to glomerular target regions in the ventrolateral central brain, covered only part of the lobula as cell populations or are VPNs of a different optic lobe region. (**A**,**B**) LC14 cells, which project to the contralateral lobula, have been previously described (***Hassan et al., 2000***; ***Otsuna and Ito, 2006***). LC14 is the name used by Otsuna and Ito; some closely related cells, here named LC14b, project to the contralateral medulla in addition to the lobula (***Hassan et al., 2000***; ***Langen et al., 2013***). LC19 (**C**) and LC23 (**D**) are newly identified cell types that project to the contralateral (LC19) or both the ipsi- and contralateral (LC23) central brain. LC19 and LC23 neurons have cell bodies in the cell body rind between optic lobe and central brain near the dorsal tip of the lobula neuropile. LC19 arbors in the lobula are located mainly in layers Lo5 and Lo6, those of LC23 neurons primarily in layers Lo2 and Lo4 (see ***Figure 5—figure supplement 1*** for details of lobula stratification). LC19 processes are present across the entire lobula; those of LC23 appear to cover only the anterior, not the posterior lobula. Images show projection views (generated in Vaa3D) of MCFO labeled neurons together with the anti-Brp neuropil marker (grey). (**E**) An example of a columnar lobula plate VPN (LPC1) also identified by others (***Panser et al., 2016***). LPC1 cells have cell bodies in the lobula plate cortex. Their processes in the lobula plate are mainly in lobula plate layer Lp2. (**A**), (**B**) and (**C**) show multiple cells; (**D**) and (**E**) segmented single cells. Scale bar represents 50 μm.

DOI: 10.7554/eLife.21022.004

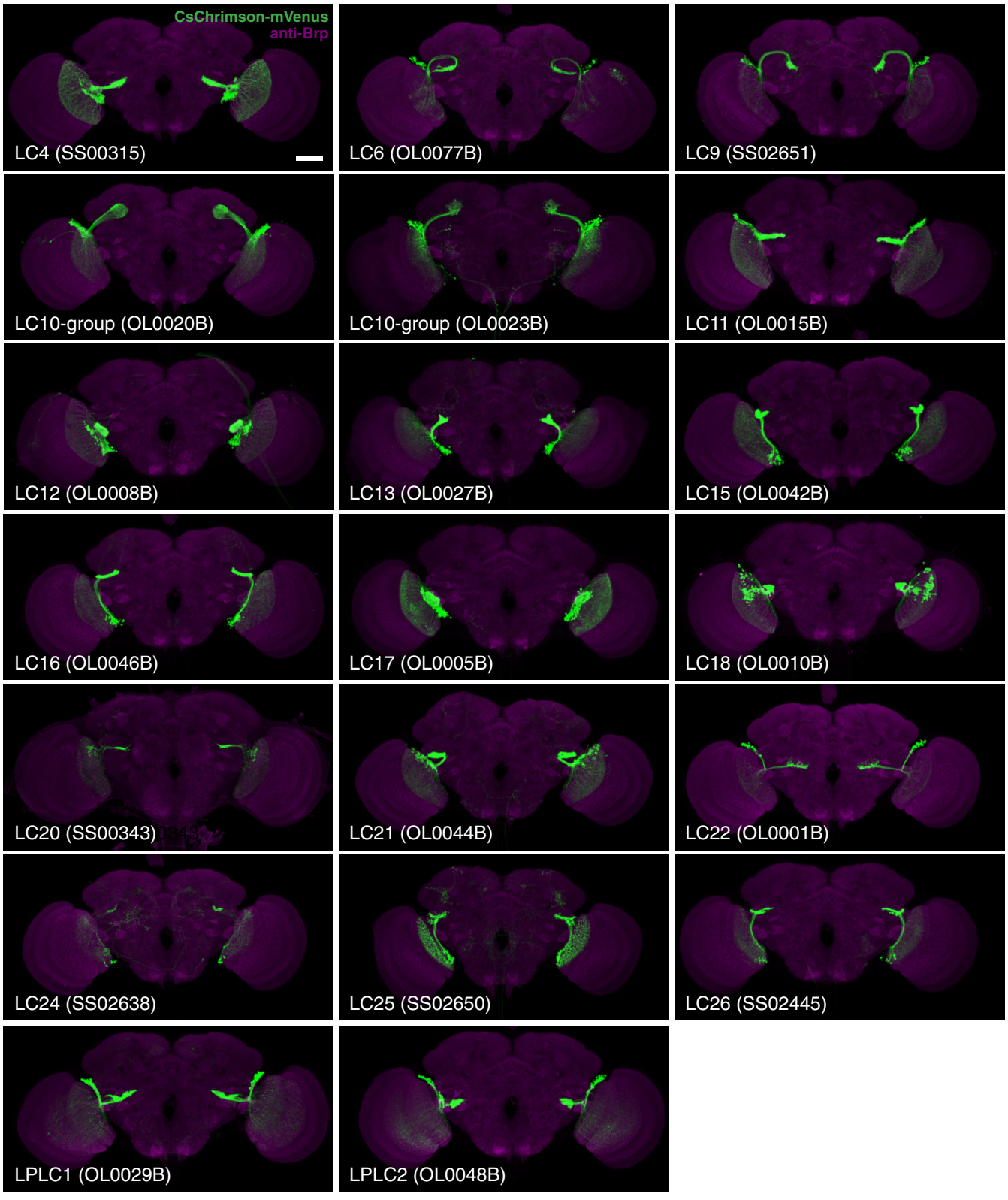

Figure 2. Expression patterns of LC neuron split-GAL4 lines. Split-GAL4 driven expression of 20xUAS-CsChrimson-mVenus (insertion in *attP18*; visualized using anti-GFP antibody labeling; green) and a neuropil marker (anti-Brp, magenta) are shown. Genotypes are identical to those used in the

Figure 2 continued on next page

Figure 2 continued

behavioral experiments in ***Figure 8***. Some adjustments of brightness and contrast of individual samples were made. For each driver line (but not across different lines), adjustments and microscope settings were identical for the brain shown in this Figure and the corresponding ventral nerve cord (VNC) shown in ***Figure 2—figure supplement 1***. The images in this and other figures with CsChrimson expression patterns are representative of 2–5 brains and 2–3 VNCs imaged for each split-GAL4 line. Scale bar represents 50 μm. Original confocal stacks are available from www.janelia.org/split-GAL4.
DOI: 10.7554/eLife.21022.005

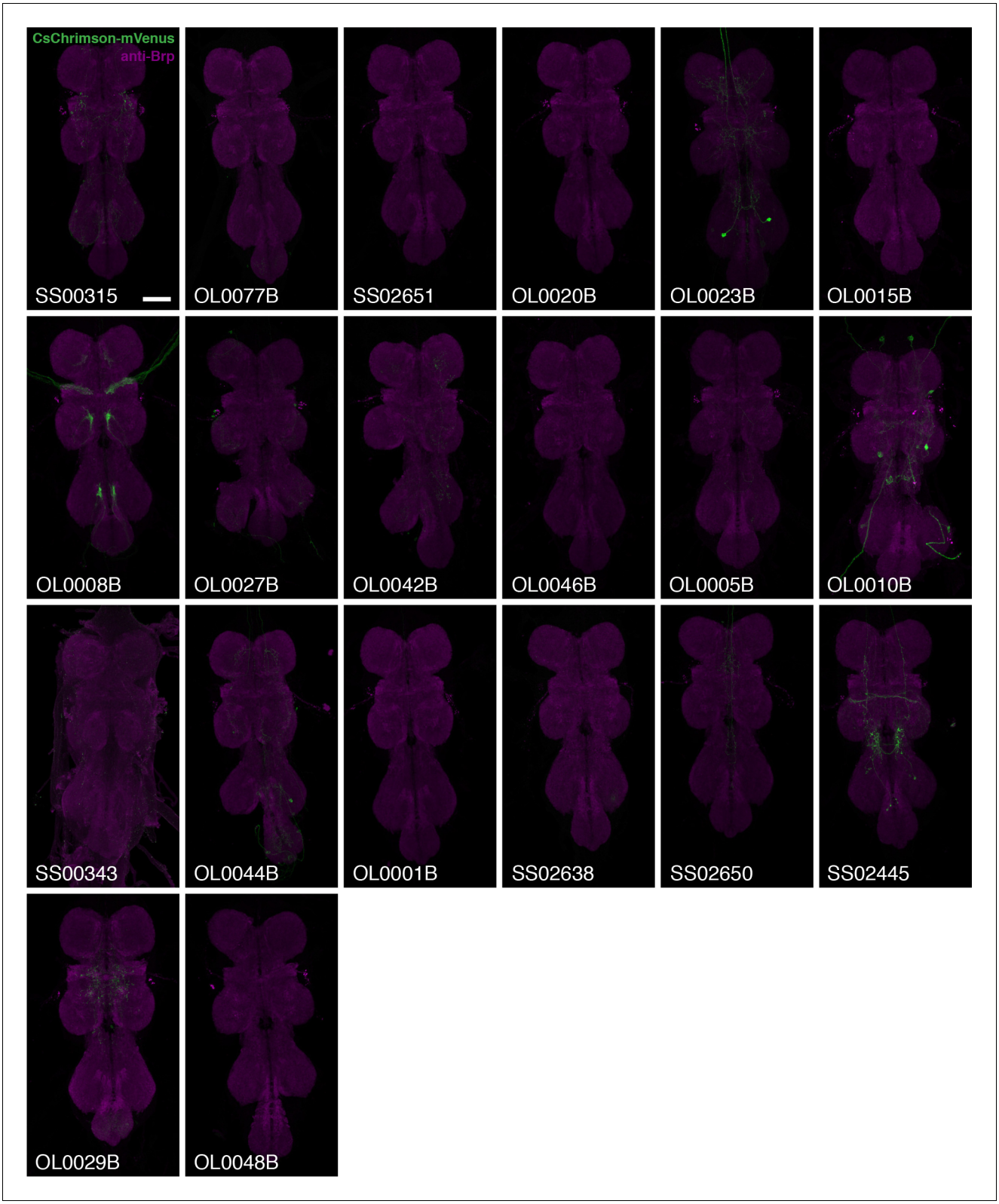

Figure 2—figure supplement 1. VNC expression patterns of the corresponding brains shown in ***Figure 2***. Imaging parameters and brightness or contrast adjustments were identical for each brain/VNC pair. Scale bar represents 50 μm. Original confocal stacks are available from www.janelia.org/split-GAL4.

DOI: 10.7554/eLife.21022.006

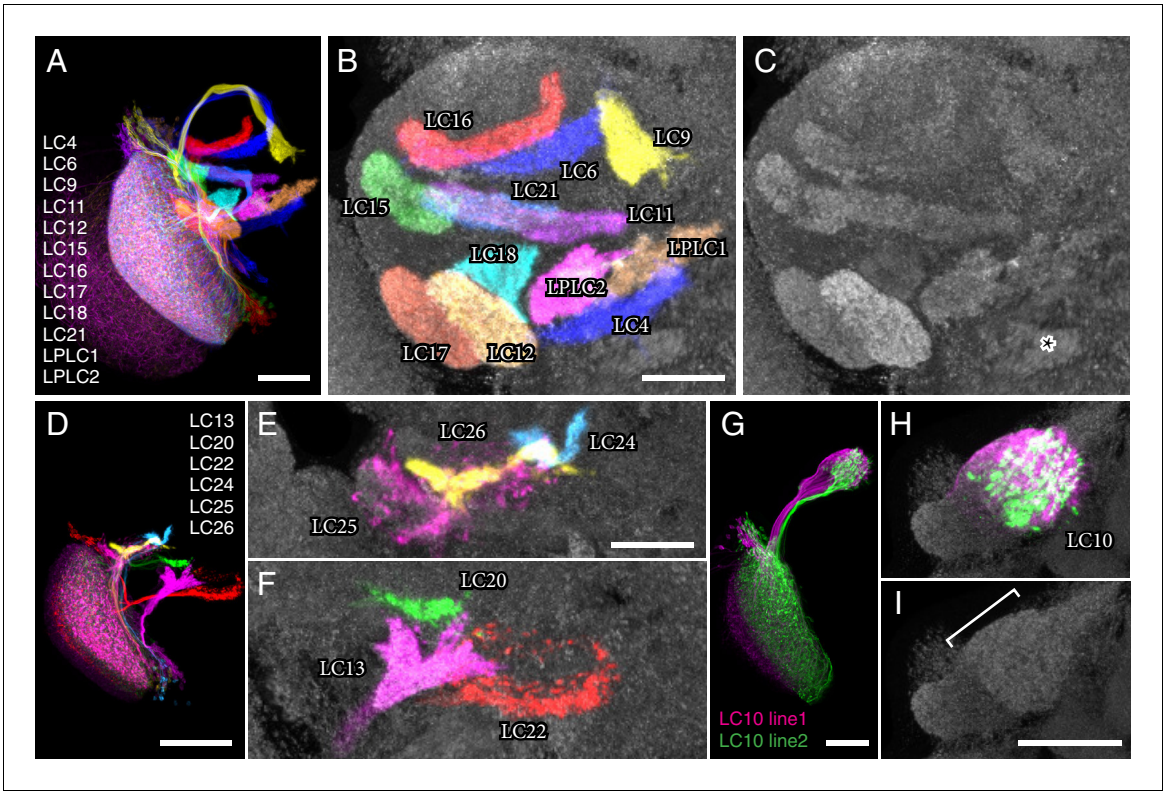

Figure 3. LC neuron terminals in the central brain are organized into distinct neuropil structures. (**A**) Illustration of the projection patterns of 12 LC cell types that project to major optic glomeruli in the PVLP (or in the PVLP/PLP boundary region). Image is a substack maximum intensity projection of a composite image stack generated from 12 computationally aligned image stacks (one for each cell type). Images were manually segmented to exclude background and some off-target cell types. Unedited pre-alignment stacks are available from www.janelia.org/split-GAL4. For details of genotypes see ***Supplementary file 1D***. (**B,C**) Target regions of the LC neurons shown in (**A**) match the optic glomeruli pattern in the PVLP. Target regions of different LC cell types were labeled by split-GAL4 driven expression of a presynaptic marker (pJFRC51-3XUAS-IVS-syt::smHA in *su(Hw)attP1*, detected using anti-HA antibody labeling). Images for different cell types were edited and combined as described above. The anti-Brp pattern of the standard brain used for alignment is shown in grey. (**C**) Pattern of optic glomeruli revealed by anti-Brp labeling. Image is the same as the anti-Brp channel of the overlay shown in (**B**). Note the close correspondence of the presynaptic terminals of LC cell populations and optic glomeruli. Asterisk marks a large synapse rich (based on anti-Brp labeling) glomerular structure in the PLP that appears to be the target of several columnar VPNs that were not included here since we considered them to be primarily associated with the lobula plate, not the lobula (though some have lobula branches). As an example, one cell of one such type (LPC1) is shown in ***Figure 1—figure supplement 1E***. LPC1 was also identified by (***Panser et al., 2016***). (**D–F**) Overlays generated as in (**A**) and (**B**) showing the projection patterns (**D**) and target regions (**E,F**) of additional LC neurons with terminals in the posterior PVLP and in the PLP. LC24, LC25 and LC26 projected to locations close to those of LC15, LC6 and LC16 but slightly more posterior and might also slightly overlap with each other. In particular, LC25 was unusual in that its terminals spread along the surface of, and perhaps partly overlapped with, the LC15 target region and other adjacent glomeruli (**E** and ***Figure 3—figure supplement 2***). Similarly, part of the boundary of the LC22 target region, as visualized by synaptic marker expression in LC22 cells, was less well defined than the boundaries of most other glomeruli (**F**). The LC22 glomerulus also appears to overlap with the target region of a second columnar VPN: stochastic labeling experiments revealed an additional LPLC-like cell type (distinct from LPLC1 and LPLC2 and tentatively named LPLC4 in agreement with [***Panser et al., 2016***]) that projects to the same approximate location as LC22. While we have yet to generate specific split-GAL4 drivers for this additional LPLC cell type and therefore did not further characterize these neurons here, their overlap with LC22 terminals was directly confirmed by co-labeling of single cells of both types in the same specimen (***Figure 3—figure supplement 1***). (**G–I**) LC10 neurons project to the large subunit of the AOTu. Overlays (generated as described above) showing cell shapes (**G**) and presynaptic sites (**H**) of LC10 cells labeled by two different split-GAL4 driver lines. LC10 neurons showed two distinct general projection paths with axons entering the large subunit of the AOTu from both dorsally and ventrally (magenta cells) or only from ventrally (green cells), in agreement with previous findings suggesting the existence of LC10 subtypes (***Otsuna and Ito, 2006***). (**I**) Anti-Brp reference pattern alone. The LC10 terminals are in a distinct large subcompartment (white bracket) of the AOTu. The AOTu also includes smaller subunits adjacent to this LC10 target region. Scale bars represent 30 μm (**A,G,I**), 20 μm (**B, E**) or 50 μm (**D**).

DOI: 10.7554/eLife.21022.007

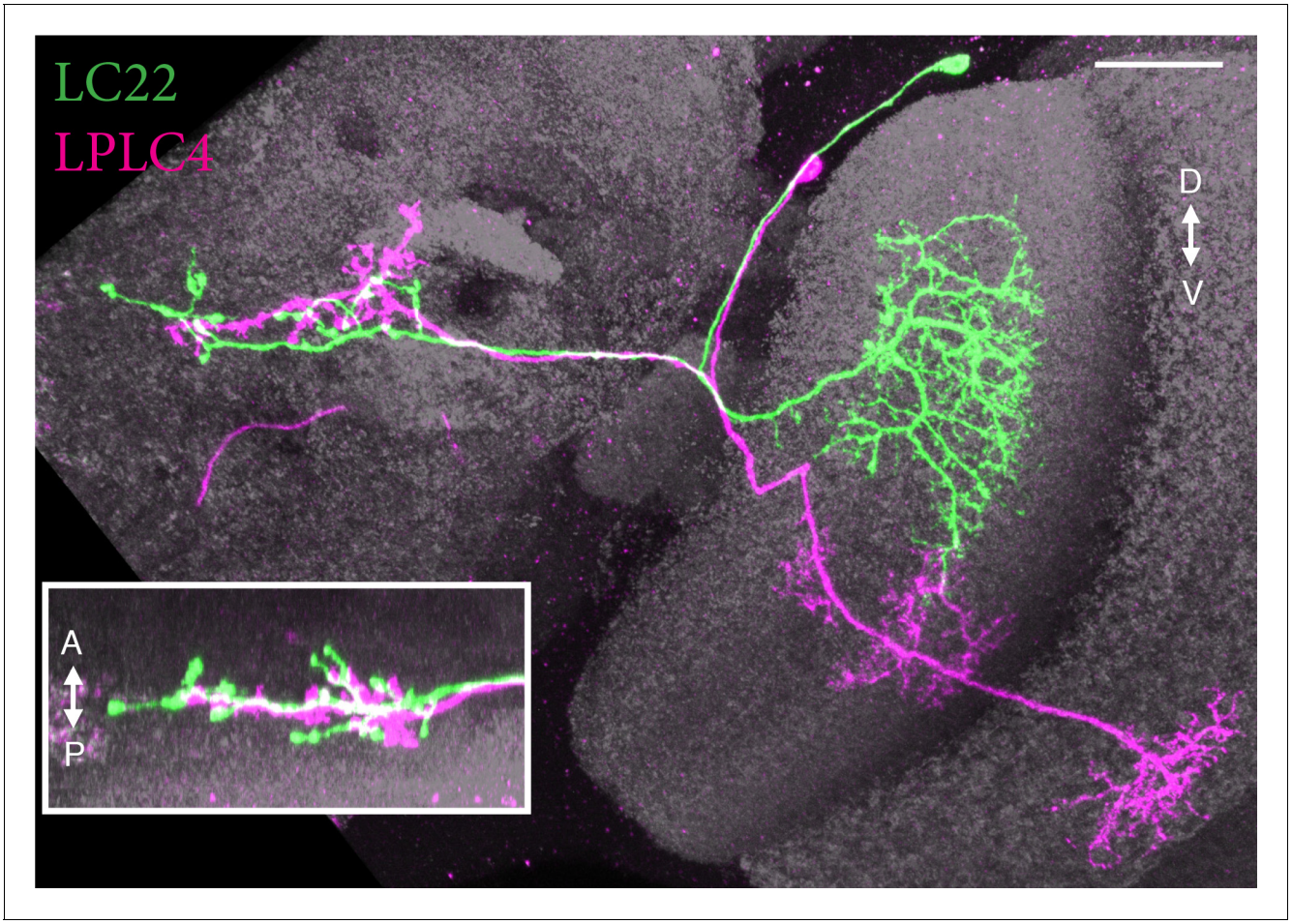

Figure 3—figure supplement 1. A second type of columnar VPN projects to the LC22 target region. Main image and inset show two views along approximately orthogonal axes of MCFO labeled LC22 (green) and LPLC4 (magenta) cells generated using a GAL4 driver line (R11C10) with expression in both cell types. The layer pattern of LPLC4 dendrites is different from both LPLC1 and LPLC2 (see ***Figure 5*** and ***Figure 7—figure supplement 2***). Images show reoriented substack projection views generated using Vaa3D. Scale bar represents 20 μm.

DOI: 10.7554/eLife.21022.008

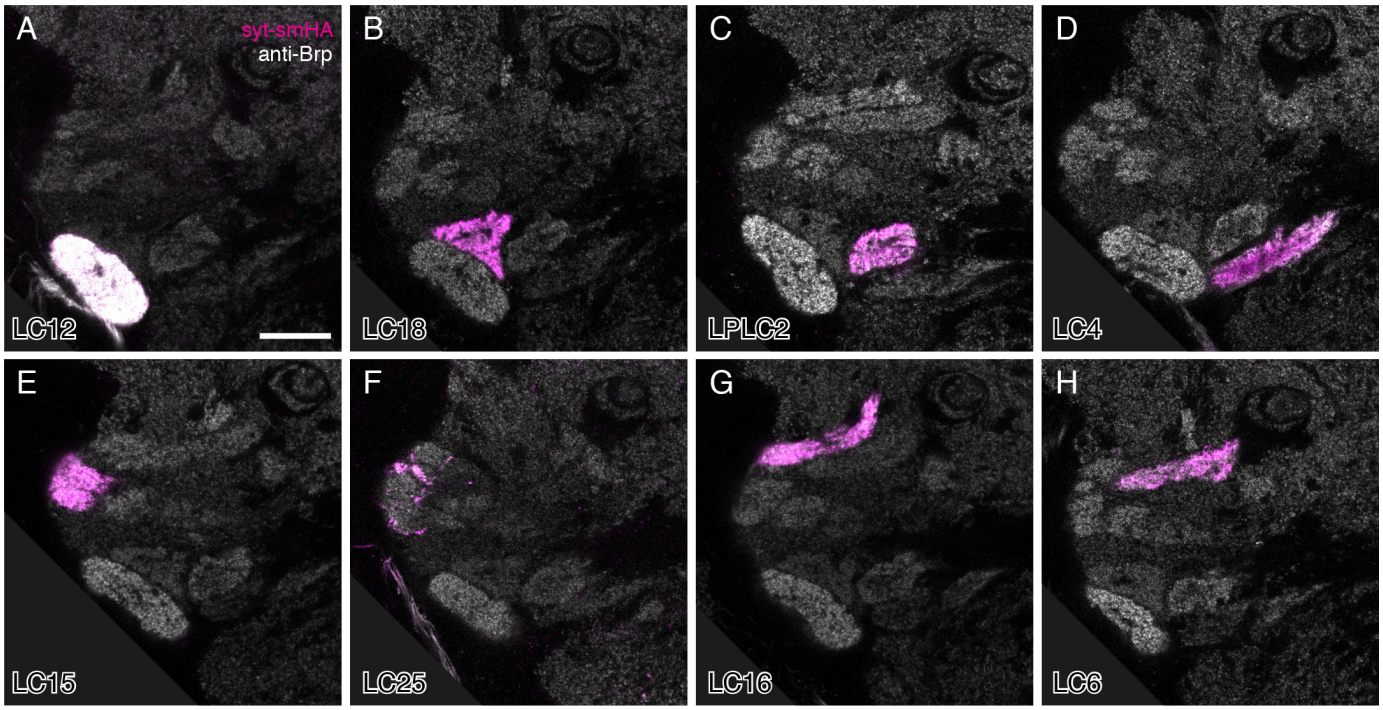

Figure 3—figure supplement 2. Presynaptic marker expression in individual LC cell types. Single confocal sections are shown. Images were rotated to show similar views. The anti-Brp reference pattern (grey) and the presynaptic marker (syt-smHA, magenta) are shown. The white appearance of the LC12 glomerulus is due to cross-talk between different labeling channels that occurred in some samples (see Materials and methods). Genotypes are the same as in the images used for the overlays in ***Figure 3***. Many LC types also show some syt-smHA labeling in the lobula; examples of this are shown in ***Figure 5—figure supplement 2*** and additional cases included in ***Supplementary file 1A***. Scale bar represents 20 μm.
DOI: 10.7554/eLife.21022.009

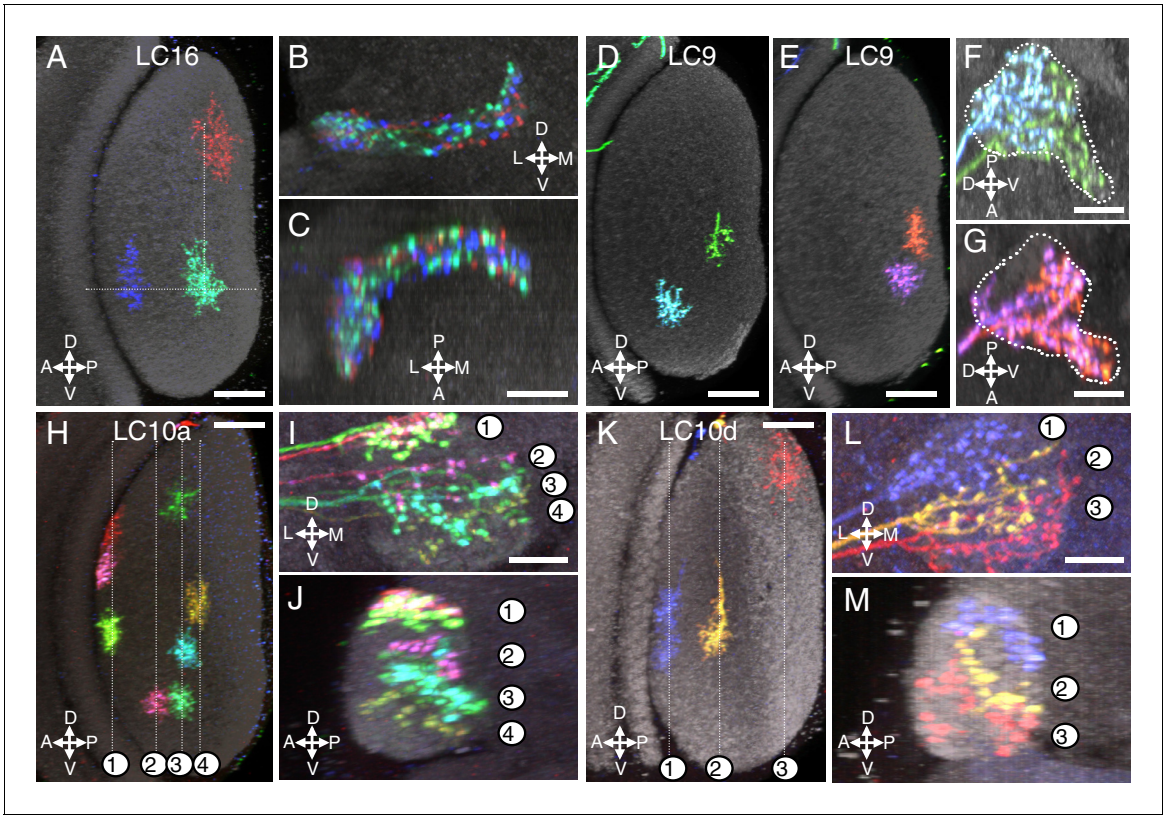

Figure 4. Multicolor stochastic labeling reveals differences in the arrangement of the terminal arbors of different LC types within their target glomerulus. (**A–C**) LC16. (**A**) Position of the dendrites of three LC16 cells in the lobula in a layer cross-section view. Each cell occupies a distinct position along the long (DV) and short (AP) axes of the lobula (dotted white lines were added to facilitate comparison of the positions of different cells). By contrast, within the target glomerulus (**B**,**C**; two roughly orthogonal views are shown) the arbors of the same cells are intermingled without an obvious correlation to the retinotopic pattern in the lobula. Most other LC types appeared similar to LC16; additional examples are shown in ***Figure 4—figure supplement 1***. (**D–G**) LC9. Most LC9 cells have presynaptic arbors that spread through more than one half of the glomerulus but do not fill it completely (**F**,**G**). Comparison of the approximate positions of arbors of individual LC9 cells in the glomerulus (**F**,**G**) with the AP positions of their dendrites in the lobula (**D**,**E**) suggests some retinotopy within the glomerulus, though with very low spatial resolution: For example, out of 57 examined LC9 cells, all of the cells (27/27) with axon terminals in the anterior-ventral tip of the glomerulus (such as the green cell in [**F**] and both cells in [**G**]) also had dendrites in the posterior half of the lobula while this was the case for only a few of the remaining LC9 cells (6/30). White dotted lines in (**F**) and (**G**) indicate the approximate boundaries of the LC9 glomerulus. (**H–M**) LC10. The relative order of LC10a (**H–J**) and LC10d (**K–M**) terminals along the DV axis of the AOTu (shown in two orthogonal views, I,J for LC10a and L,M for LC10d) matches the order along the AP axis of the lobula (H for LC10a and K for LC10d). Individual cells were labeled using MCFO. Reconstructed views of reoriented subtstacks generated in Vaa3D are shown. For both LC10a and LC10d, similar results were observed for LC10 cells from five optic lobes, each with at least three labeled cells. Analyses of MCFO-labeled LC10b (36 cells from 18 brains) and LC10c (33 cells from 17 brains) single cells also showed an approximate correspondence between AP positions of dendrites in the lobula and DV positions of axonal arbors in the AOTu. LC10b cells also showed considerable variation in their lateral-medial spread within the medial zone of the AOTu but further analyses will be required to explore possible correlations between these differences and arbor positions in the lobula. Scale bars represent 20 μm (**A**,**D**,**E**,**H**,**K**) or 10 μm (**C**,**F**,**G**,**I**,**L**).

DOI: 10.7554/eLife.21022.010

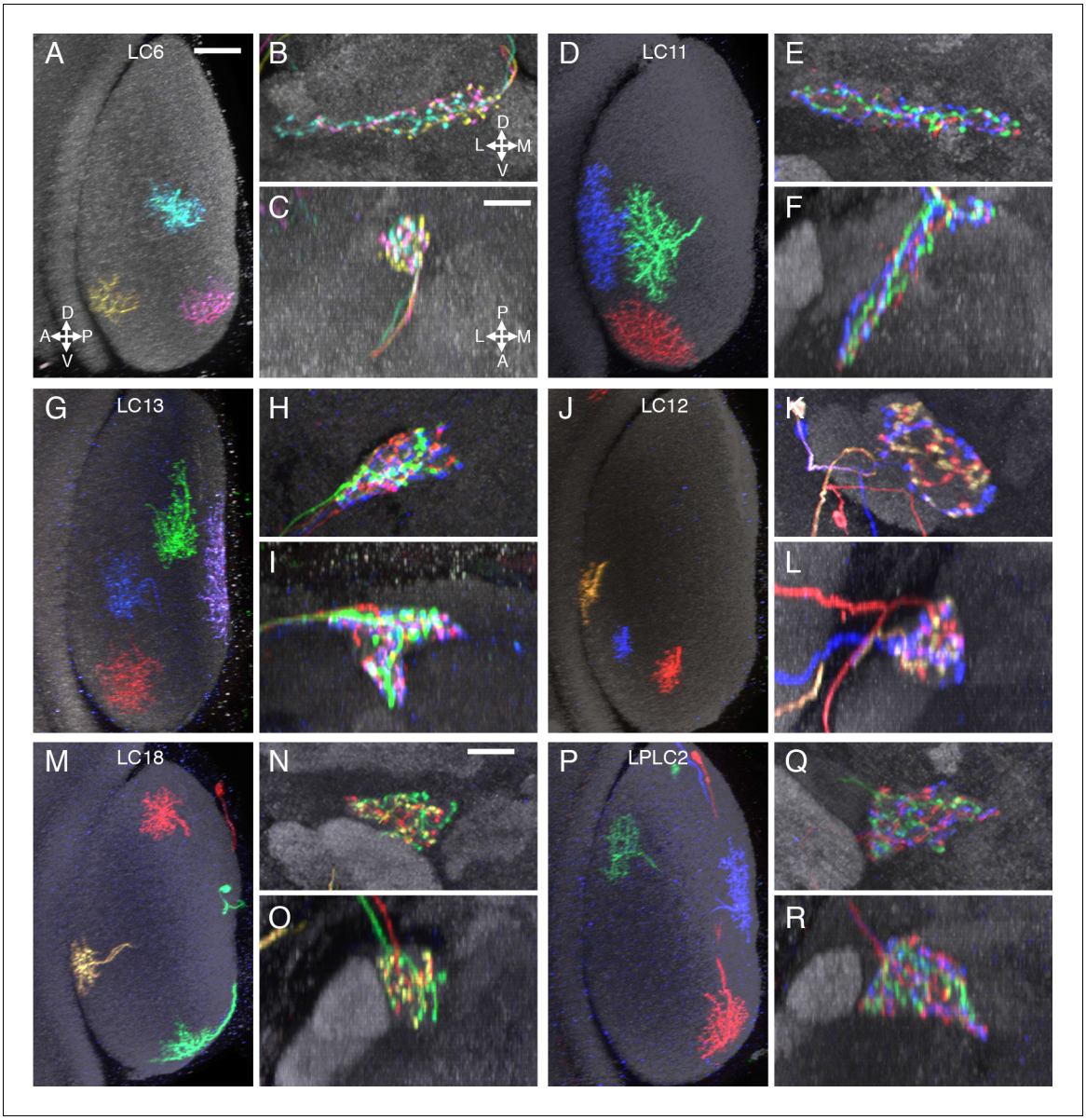

Figure 4—figure supplement 1. Terminal arbor arrangements of additional LC cell types. (**A–C**) LC6, (**D–F**) LC11, (**G–I**) LC13, (**J–L**) LC12, (**M–O**) LC18, (**P–R**) LPLC2. Substantial overlap of the arbors of co-labeled single cells in their target regions was also observed for the remaining LC cell types (at least two brains with two or more labeled cells were examined for each cell type). While there are occasional differences between the spread of single cells of the same type within their target glomerulus (e.g. the LC6 cells in (**B**) do not all extend to the lateral tip of the glomerulus), we did not find obvious correlations between such differences and these cells' retinotopic positions in the lobula. Lobula cross-section views and two orthogonal views of the target glomerulus are displayed as in ***Figure 4***. Scale bars represent 20 μm (**A**) or 10 μm (**C**).

DOI: 10.7554/eLife.21022.011

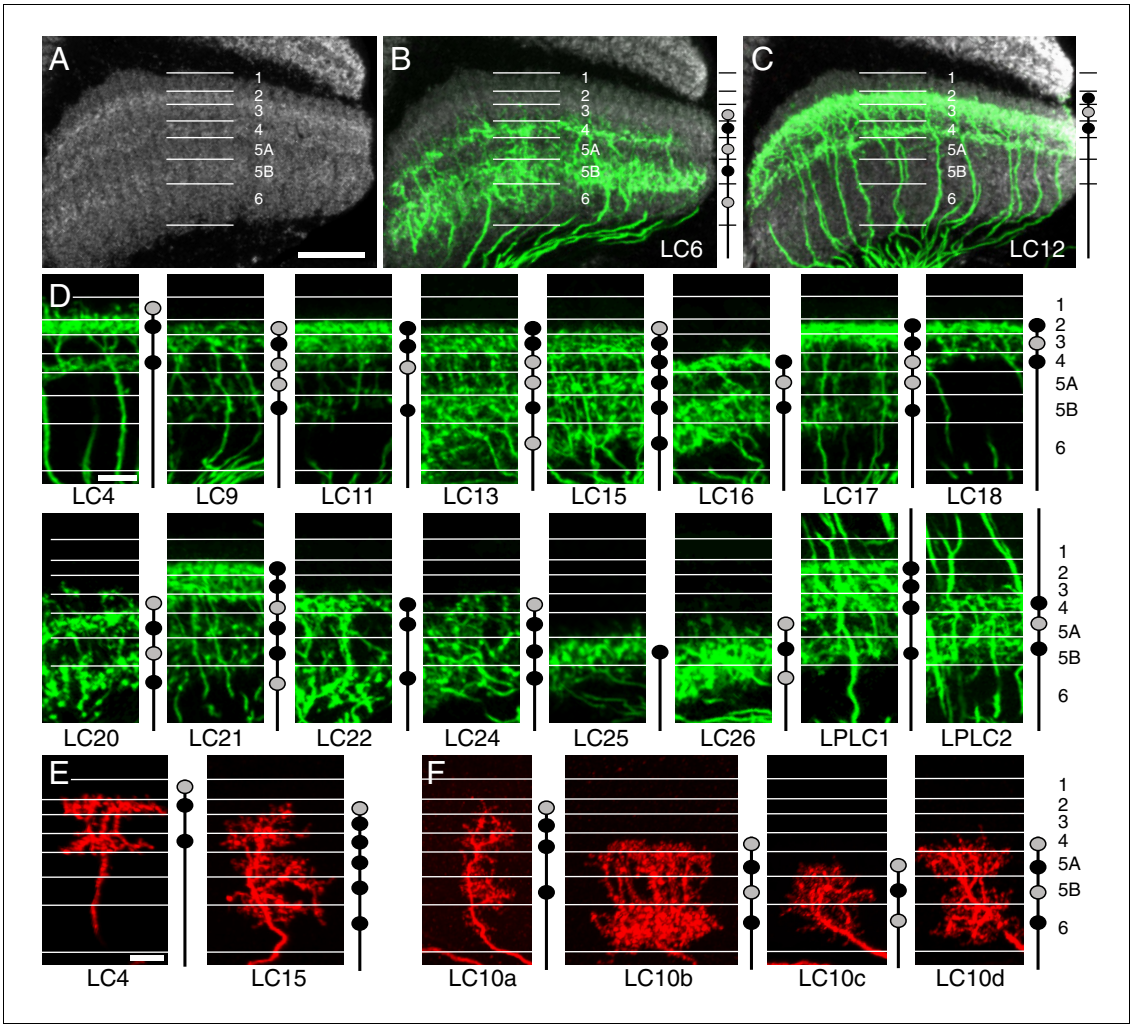

Figure 5. Layer specific arborizations of LC neurons in the lobula. (**A**) Anti-Brp neuropil marker shows bands of different intensity in the lobula that can serve as approximate markers of layer boundaries. The image is a maximum intensity projection through 10 adjacent sections (0.38 µm spacing) of the reference channel of the standard brain used for alignments. Approximate layer boundaries are indicated. Layer boundaries were defined by the positions of known cell types and closely match the anti-Brp pattern (see ***Figure 5—figure supplement 1***). Lo5 was divided into two sublayers based on the anti-Brp pattern. Further subdivisions of strata based on the positions of arbors of different cell types would be possible but were not applied here. (**B**,**C**) Layer patterns of LC6 (**B**) and LC12 (**C**). Split-GAL4 expression of a membrane marker is shown in green. Images were aligned to a standard brain using the anti-Brp pattern (shown in grey). Images are maximum intensity projections through the same series of sections of brains aligned to the same template as in (**A**). Approximate layer boundaries are marked with white lines. (**D**) Layer patterns of the remaining LC cell types (except LC10 neurons). Projections were generated as in (**B**,**C**) but are shown without the anti-Brp pattern. All layers, but only a portion of the lobula is shown. Schematics in (**B–F**) indicate innervated layers as filled circles; black circles represent more extensive arborizations than grey circles. Note that these simplified schematics do not capture some details of the layer patterns (such as sublayer patterns). An additional description of layer patterns can be found in ***Supplementary file 1A***. (**E**) Single cell layer patterns are consistent with layer patterns seen at the population level. LC4 and LC15 are shown as examples. Additional single cell images can be found in ***Figure 7—figure supplement 1***. (**F**) Layer patterns of LC10 subtypes. LC10b and LC10d cells have similar layer patterns but differ in other aspects such as arbor size (LC10b arbors in the lobula are larger). Additional examples of MCFO labeled LC10 cells of different subtypes can be found in ***Figure 7—figure supplement 1*** and ***Figure 10—figure supplement 2***. Images in (**E**,**F**) were manually matched to the layer markers using the anti-Brp pattern. The scale of some images was slightly adjusted to compensate for varying depth of the lobula. Scale bars represent 20 µm (**A**, also applies to **B** and **C**) or 10 µm (**D**,**E**; scale bar in **E** also applies to **F**).
DOI: 10.7554/eLife.21022.012

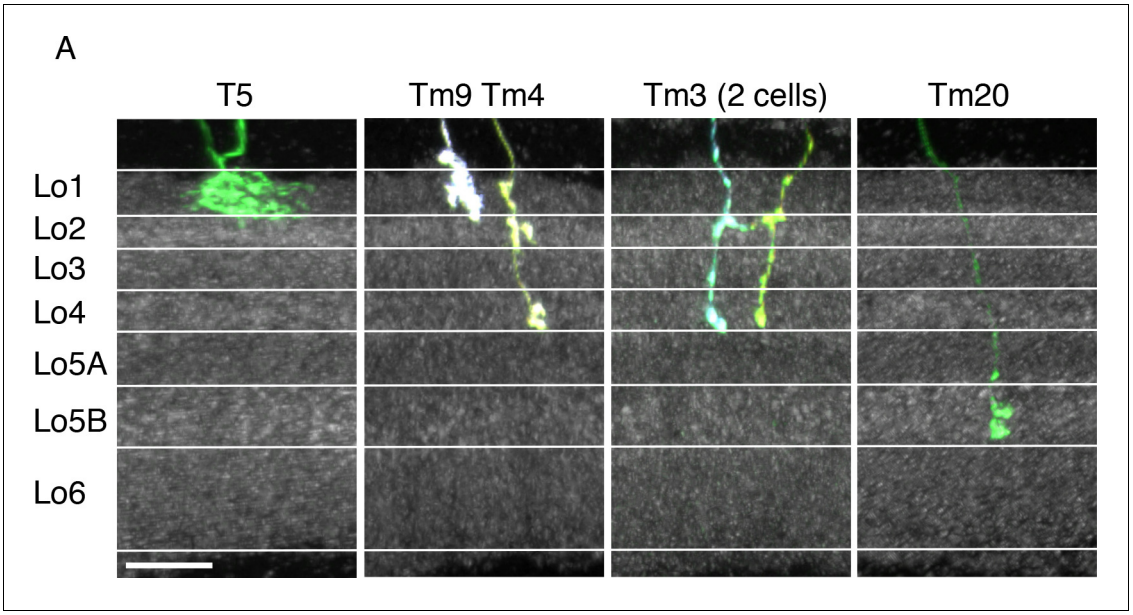

Figure 5—figure supplement 1. Layer positions of arbors of known cell types. Lobula terminals of MCFO labeled T5, Tm9, Tm4, Tm3 and Tm20 cells (***Fischbach and Dittrich, 1989***) are shown. Anti-Brp pattern is in grey. Layer boundaries are marked with white lines. Golgi studies (***Fischbach and Dittrich, 1989***) have described T5 and Tm9 in Lo1, Tm4 and Tm3 proximal terminals in Lo4 near the boundary of Lo5, and Tm20 terminals in Lo5 near the boundary of Lo6. Tm4 and Tm3 also have apparent presynaptic varicosities in Lo2 (both) and Lo1 (Tm4). These cell types therefore can be used to identify the approximate boundaries of all six lobula strata. Further division of Lo5 into two sublayers is suggested by the anti-Brp pattern and supported by the differential presence of arbors of several neuronal cell types in these sublayers (compare for example, LC20 and LC25 in ***Figure 5D***). Images show reoriented substack projection views generated using Vaa3D. Scale bar represents 10 μm.
DOI: 10.7554/eLife.21022.013

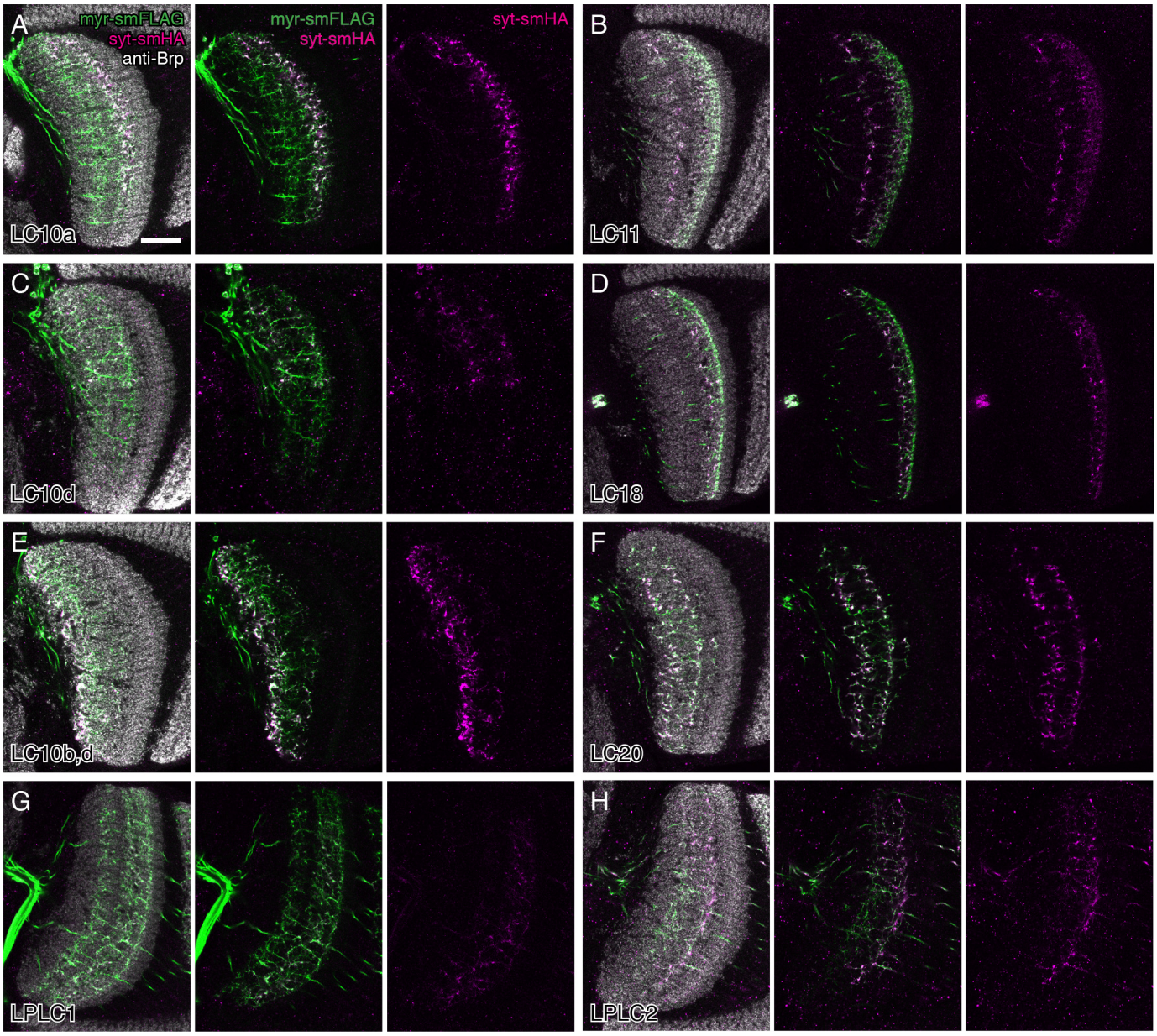

Figure 5—figure supplement 2. Potential presynaptic sites of LC neurons in the lobula. In addition to the target glomerulus in the central brain (see ***Figure 3*** and ***Figure 3—figure supplement 2***), split-GAL4 driven pJFRC51-3XUAS-IVS-syt::smHA in *su(Hw)attP1* expression also resulted in labeling in the lobula in several LC cell types. Single confocal sections with anti-Brp in grey, syt-smHA in magenta and/or a membrane marker (pJFRC225-5XUAS-IVS-myr::smFLAG in *VK00005*) in green are shown for each cell type as indicated in (**A**). Although the interpretation of such fainter syt-smHA labeling patterns is not always straightforward, they strongly suggest that at least some LC neurons (including cell types not shown in this Figure) also have presynaptic sites within the lobula. Additional details on syt-HA labeling in the lobula are provided in ***Supplementary file 1A***. Strong syt-smHA labeling in layer Lo6 in (**E**) appears to be mainly due to LC10b cells (compare with (**C**) for LC10d cells alone), though a lobula intrinsic neuron type weakly labeled by the split-GAL4 driver line used might also contribute to the pattern. Scale bar represents 20 μm.
DOI: 10.7554/eLife.21022.014

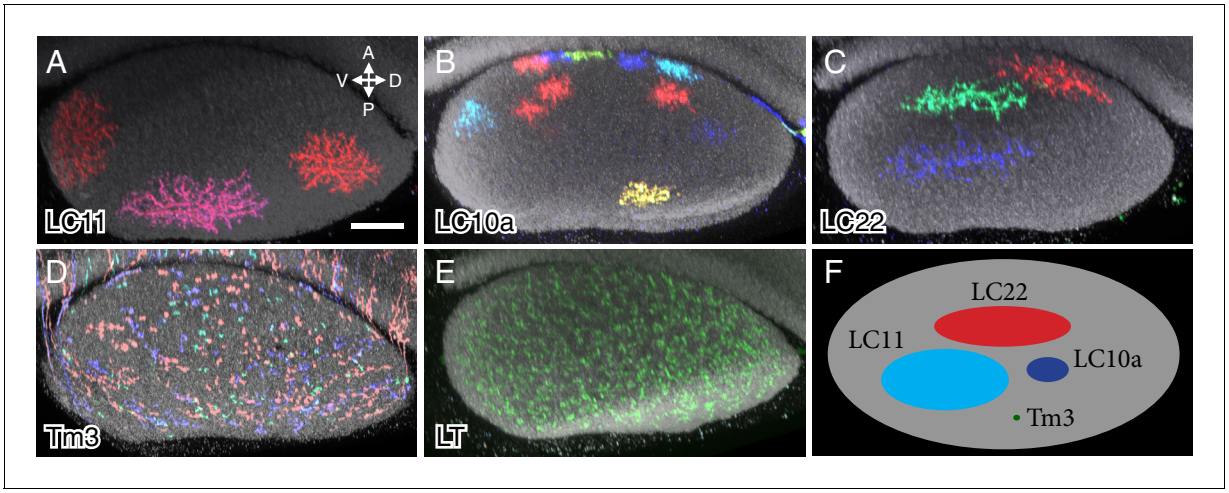

Figure 6. Column spread of LC neurons and other cell types in the lobula in cross-section views. Cells were labeled using MCFO. Cross-section views of the lobula were generated using Vaa3D. The AP and DV axes of the lobula are indicated. Anti-Brp reference marker is shown in grey. LC neuron arbor sizes and shapes in the lobula are diverse across different cell types but similar within each type. LC cell types shown are LC11 (**A**), LC10a (**B**) and LC22 (**C**). The remaining LC cell types are shown in ***Figure 6—figure supplement 1***. MCFO labeled cells of a columnar medulla neuron type (Tm3) present in each of ~750 visual columns (**D**) and a lobula tangential cell (LT) that spans the entire lobula (**E**) are shown for comparison. All LC arbors are multicolumnar with estimated sizes from about 10 (LC10a) to over 60 (LC11) visual columns. LC22 cells were similar in size to LC11 along the long (DV) but not the short (AP) axis of the lobula. (**F**) Schematic summary of the column spread of different cell types in the lobula. Scale bar represents 20 μm.
DOI: 10.7554/eLife.21022.015

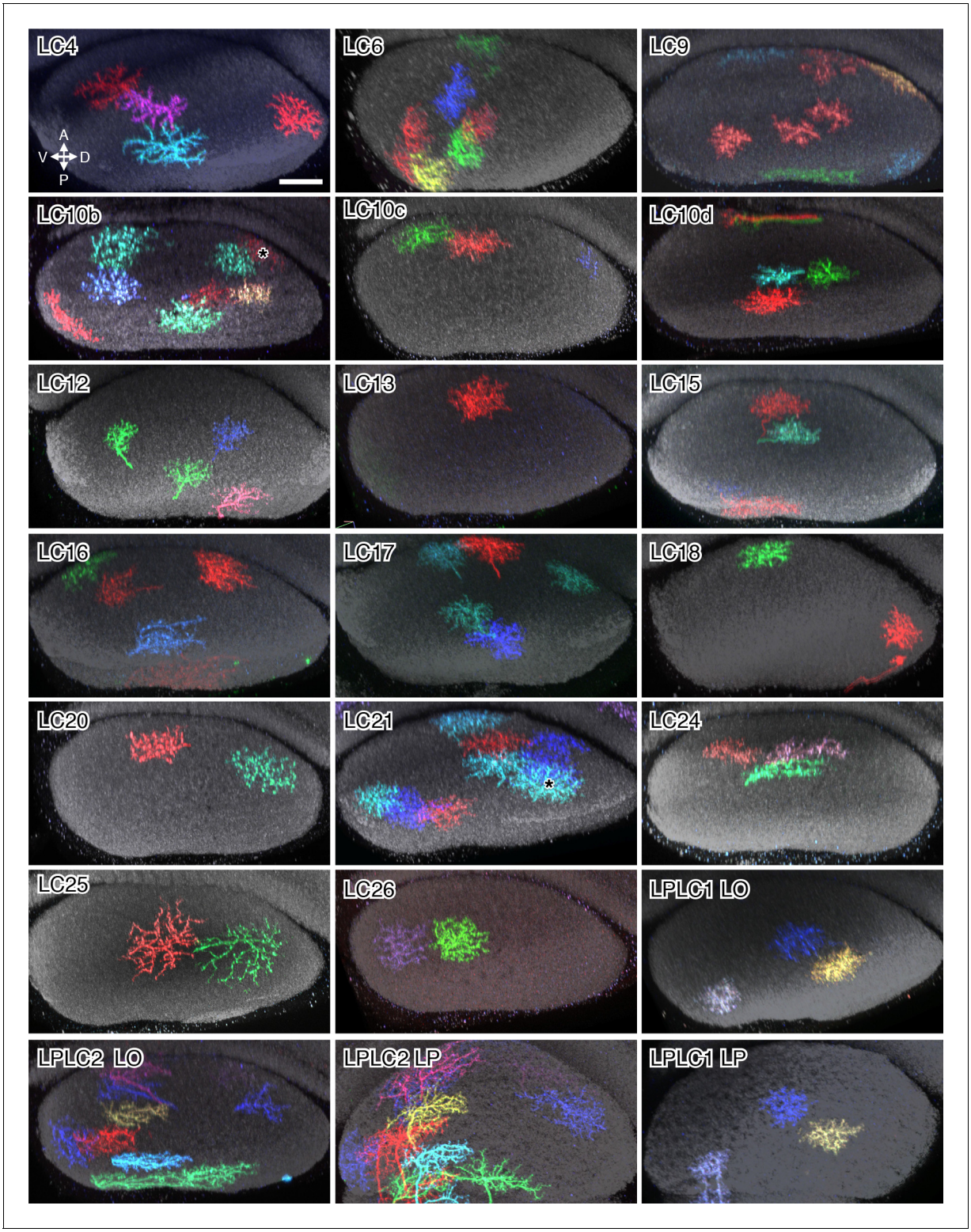

Figure 6—figure supplement 1. Layer cross-section views of lobula arbors of the LC neuron types not shown in ***Figure 6***. Cross-section views of LC cells of the indicated types were generated as described in the ***Figure 6*** legend. Asterisks in the LC10b and LC21 panels mark two MCFO labeled cells (LC10c and LC11, respectively) that do not belong to the indicated cell type. LO and LP in the LPLC panels indicate cross-section views of the lobula and lobula plate, respectively. Scale bar in the LC4 panel represents 20 μm; images of other cell types are shown at very similar scale.
DOI: 10.7554/eLife.21022.016

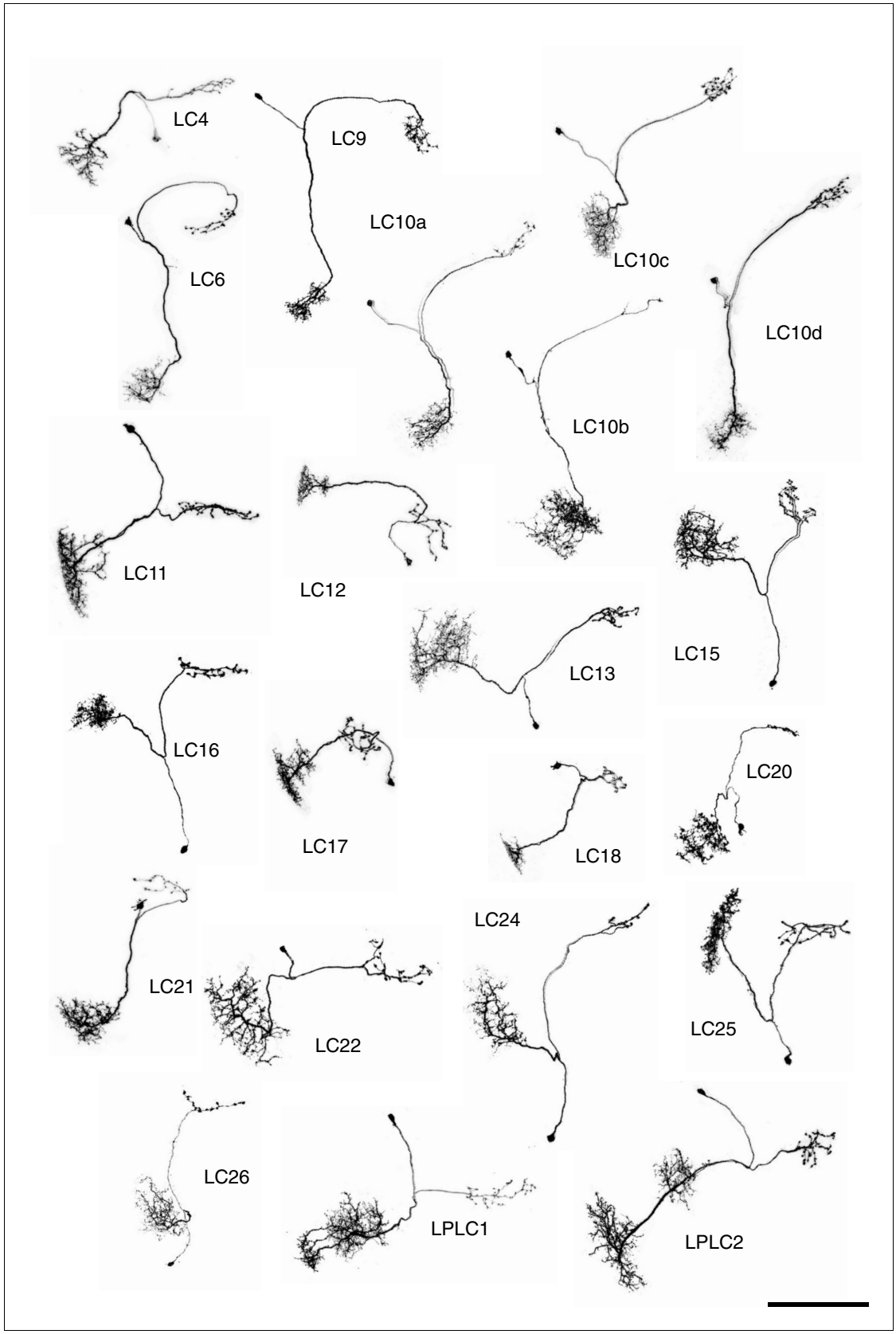
LC4
LC9
LC10a
LC6
LC10c
LC10d
LC10b
LC11
LC12
LC13
LC15
LC16
LC17
LC18
LC20
LC21
LC22
LC24
LC25
LC26
LPLC1
LPLC2

Figure 7. Single cell shapes of LC neurons. Maximum intensity projection images of MCFO labeled single cells were manually segmented to exclude other labeled cells or background signal and converted to inverted grayscale images. Cells are shown in a similar orientation (with dorsal approximately up and lateral approximately to the left) and at the same scale. Scale bar represents 50 μm.
DOI: 10.7554/eLife.21022.017

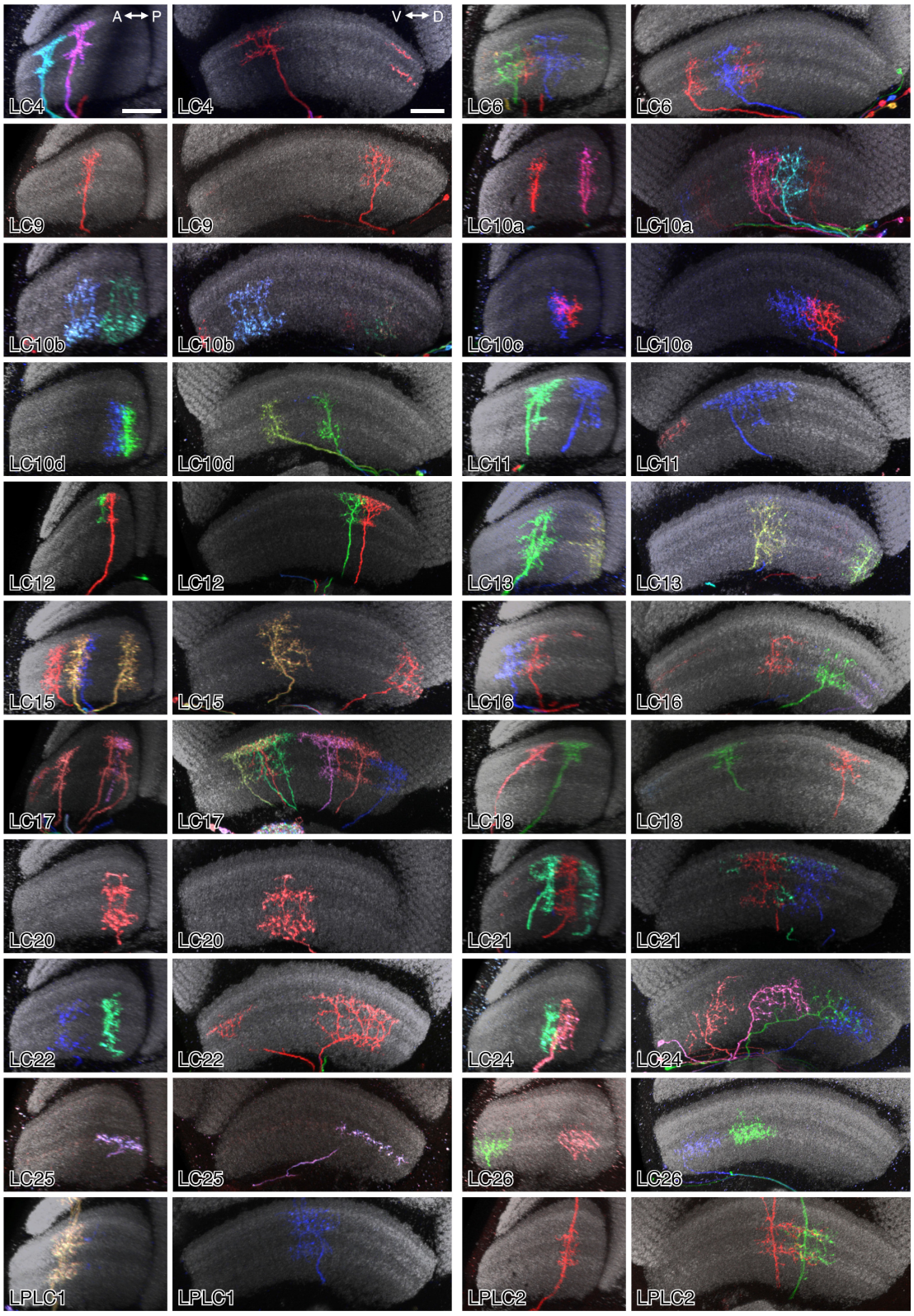

Figure 7—figure supplement 1. Layer patterns of single cells of 22 LC neuron types. Images are reoriented views (generated using Vaa3D) of MCFO labeled LC neurons. Anti-Brp neuropil marker is in grey. For each cell type, two different views, along the AP and along the DV axes of the lobula,

Figure 7—figure supplement 1 continued on next page

Figure 7—figure supplement 1 continued

respectively, are shown. The two panels for a cell type can either show the same specimen in two views or two different specimens. Scale bars in the LC4 panels represent 20 μm; images of other cell types are shown at very similar scale.

DOI: 10.7554/eLife.21022.018

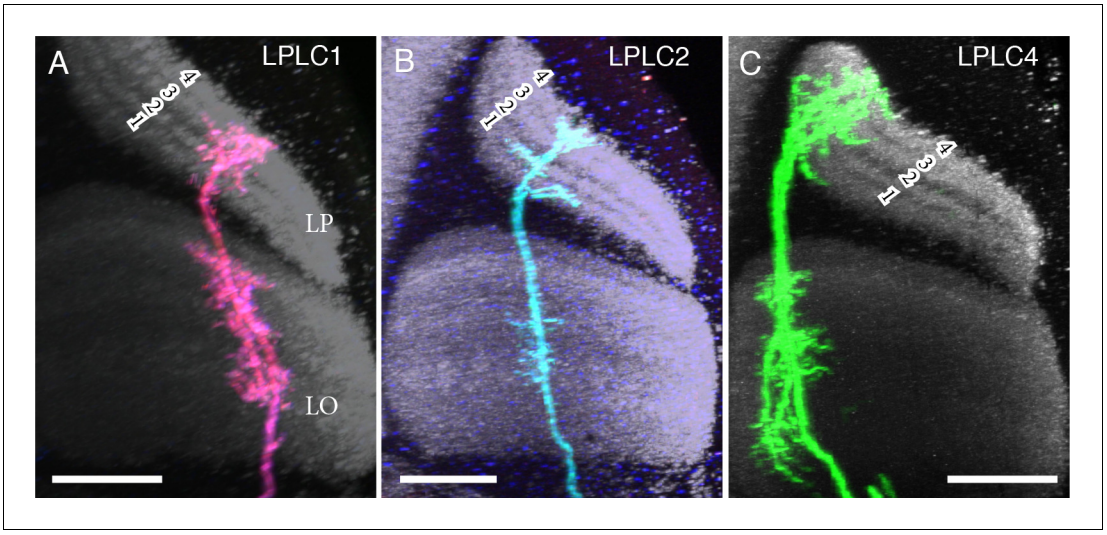

Figure 7—figure supplement 2. Single cell labeling of LPLC arbors in lobula and lobula plate. (**A**) LPLC1. (**B**) LPLC2. (**C**) LPLC4. Numbers indicate the four LP layers (***Fischbach and Dittrich, 1989***). Similar to lobula layers, the LP layers can be identified by changes in the intensity of anti-Brp labeling: Each LP layer shows a band of strong anti-Brp signal flanked by weaker labeling. All three LPLC cell types have processes in all lobula plate layers and several layers of the lobula but differ in details of arbor structure and layer patterns. For example, lobula layers of LPLC4 (mainly Lo2, Lo4 and Lo6) are different from both LPLC1 (Lo2-Lo4 and Lo5B) and LPLC2 (Lo4 and Lo5B). The presence of processes in multiple lobula plate layers, as shown by all LPLC types, could support responses to stimuli that combine different directions of motion, such as a visual loom (***Schilling and Borst, 2015***). Scale bars represent 20 μm.

DOI: 10.7554/eLife.21022.019

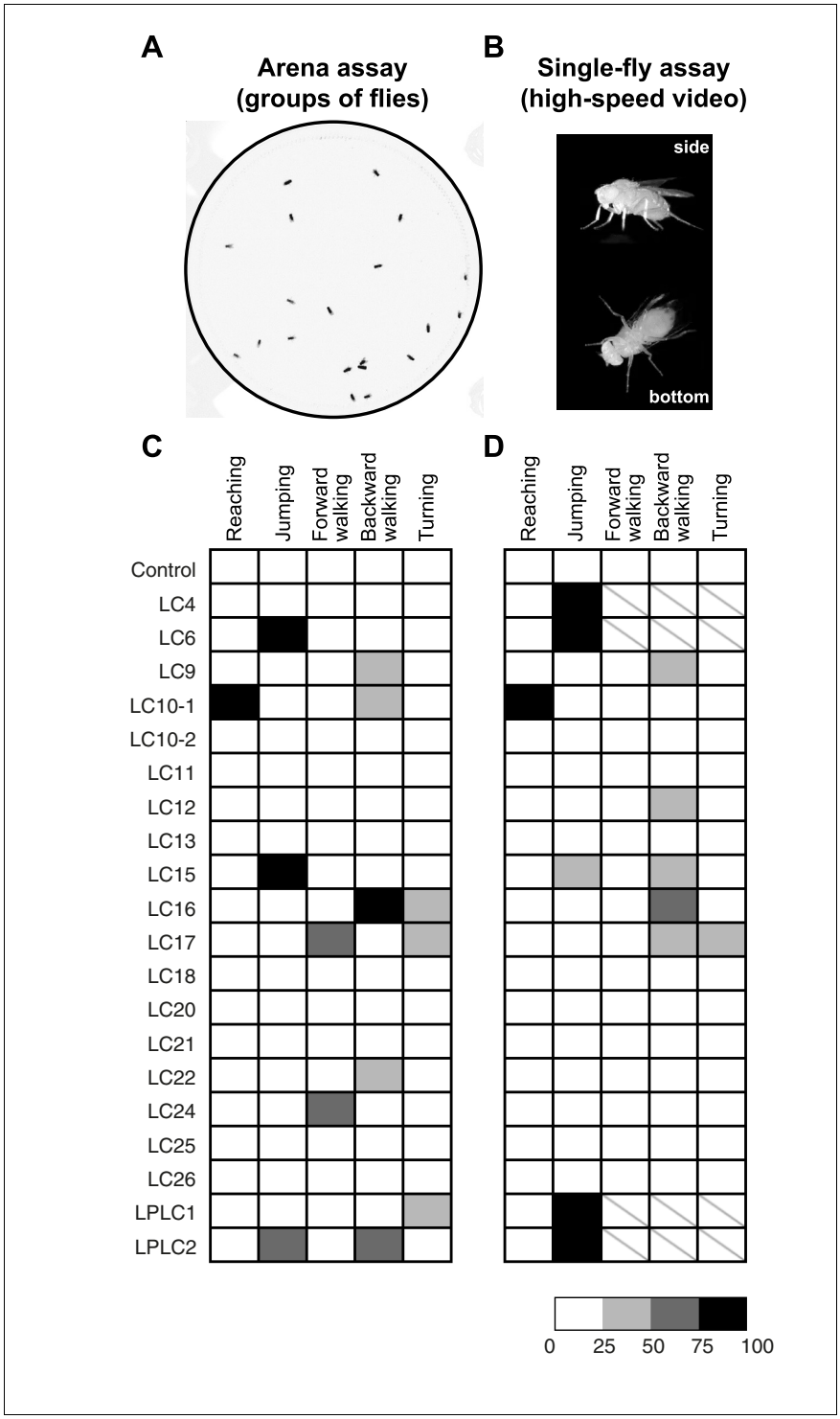

Figure 8. Optogenetic activation of LC neurons induces distinct behavioral responses that differ between LC cell types. (**A**) A representative video image of group of freely walking flies in the circular arena assay. (**B**) Representative video images of a freely behaving fly on a small glass platform in the single-fly assay. A side view (upper part of the panel) and a bottom view (lower part) of the fly are simultaneously recorded on a single high-speed video camera with the aid of two small prisms (see Materials and methods). (**C,D**) The results of CsChrimson activation of different LC cell types in the arena (**C**) and the single-fly (**D**) assays are summarized in a grayscale intensity map. Each column represents a distinct behavior and each row represents a different split-GAL4 driver line with a predominant expression in the indicated cell type. Shading represents the behavioral penetrance

Figure 8 continued on next page

Figure 8 continued

(percentage of trials or flies of a specific genotype in which a given behavior was observed, see ***Supplementary file 1B*** for the names of the GAL4 lines used and penetrance values). In both assays, the occurrences of reaching and jumping behaviors were annotated manually, while locomotor behaviors including forward walking, backward walking and turning were determined based on velocity and angular speed derived from automated fly tracking (see ***Figure 8—figure supplement 1***, and Materials and methods). For locomotor behaviors we set a conservative threshold of two standard deviations away from the mean to be considered an activation phenotype (***Figure 8—figure supplement 1E,F***). In this way, we determined the behavioral penetrance for five phenotypes – reaching, jumping, forward walking, backward walking and turning - in both the arena and the single-fly assays. In the single-fly assay, the high jumping penetrance of four LC cell types (LC4, LC6, LPLC1 and LPLC2) resulted in too few flies (<= 12) available for analyses of walking and turning behaviors (indicated with a '\').

DOI: 10.7554/eLife.21022.020

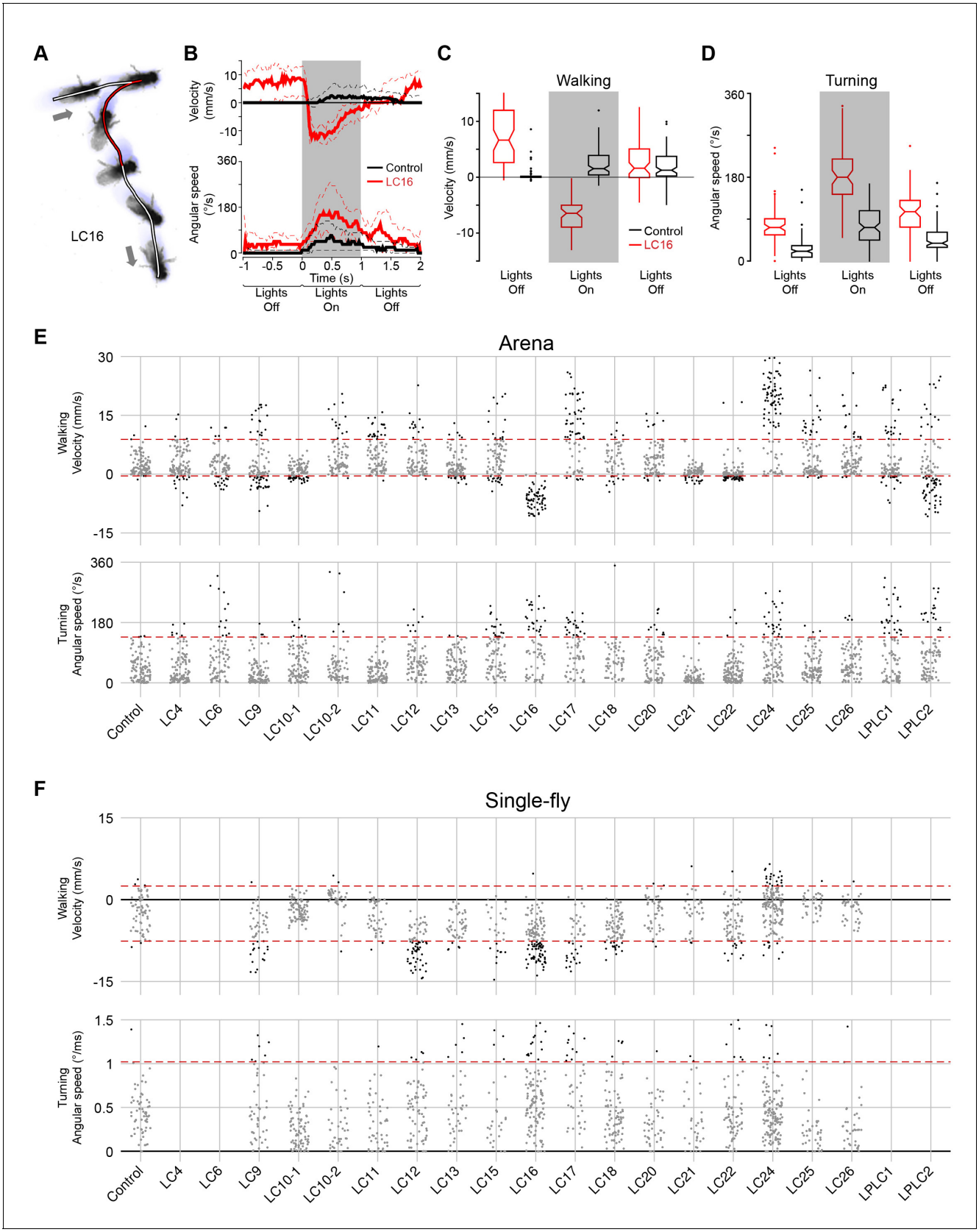

Figure 8—figure supplement 1. Quantification of locomotor behaviors and determination of behavioral penetrance. (**A**) A representative tracking of a fly with LC16 activation in the arena assay. Arrows indicate the start and end positions. Fly's trajectory is denoted in red (during stimulation, 1 s) or in

Figure 8—figure supplement 1 continued on next page

Figure 8—figure supplement 1 continued

white (before and after stimulation, 1 s each). (**B**) Time-series plot of velocity and angular speed of pBDPGAL4U control (black, trial count = 109, fly count = 23) and LC16 activated (red, trial count = 65, fly count = 14) flies. Solid and dashed lines indicate median and inner-quartile range, respectively. Grey rectangles in this and other panels signify optogenetic stimulation with red light. (**C,D**) Notched box plots showing the distribution of mean velocity (**C**) and angular speed (**D**), before, during, and after optogenetic stimulation, of pBDPGAL4U control (black) and LC16 activated (red) flies. The increased translational velocity of LC16 flies compared to controls prior to CsChrimson stimulation appears to be due to reduced walking of the control flies after repeated red light stimulation: The data in (**B–D**) are averages from multiple trials (trials 1 to trial 5) with the maximum light stimulus from experiments with increasing intensities (i.e. the same flies were stimulated repeatedly within an experiment with a series of light intensities; see Materials and methods). To examine whether the apparent higher basal locomotion of LC16 flies during pre-stimulation light off was a response to prior stimulations, we compared trial 1 data to trial 5 data from the experiments in ***Figure 9***, because in these experiments only the maximum light stimulus was used (data for different LC16 split- GAL4 lines and for the different control flies shown in ***Figure 9*** were pooled). Data for trial 1 showed no pre-stimulus difference between LC16 and control flies ($p=0.88$, by Wilcox rank sum test), while locomotion was reduced for the controls in trial 5 ($p<0.01$). (**E,F**) Jitter plots showing the distribution of mean velocity and angular speed during optogenetic stimulation of control and LC neuron driver lines in the arena (**E**) and single-fly (**F**) assays. Each dot represents an individual trial. A conservative threshold is set at the 97.7th percentile of the pBDPGAL4U control distribution, indicated by dashed red lines. Grey and black dots represent trials within and outside of the normal range, respectively. For walking, trials above the top red line are counted as displaying a forward walking phenotype and trials below the bottom red line are counted as displaying a backward walking phenotype. For turning, trials above the red line are counted as displaying a turning phenotype.
DOI: 10.7554/eLife.21022.021

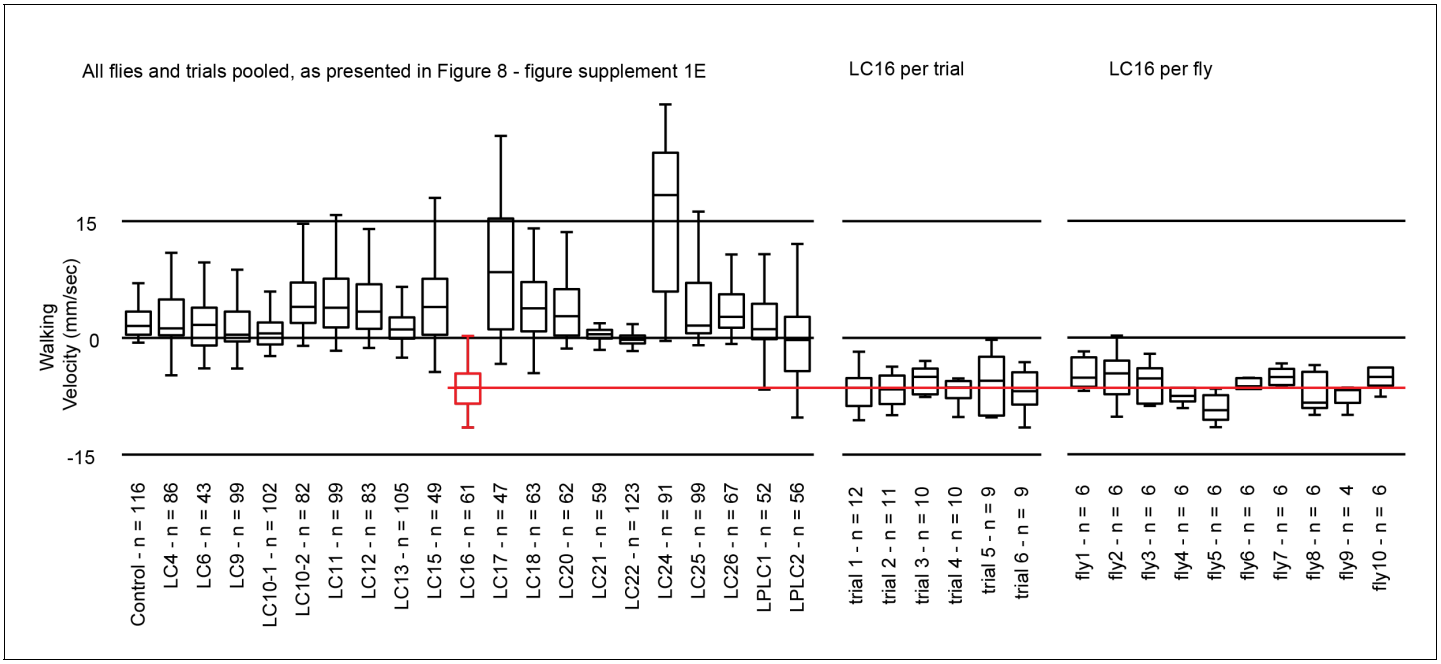

Figure 8—figure supplement 2. Variability of LC16 backward walking behavior across trials and across flies. In the circular arena experiments, each fly was repeatedly tested in a series of trials (see Materials and methods). For most analyses, we pooled data across all flies and trials (as shown in the left panel for walking behavior after optogenetic stimulation of different LC neuron types; these are the same data plotted as a separate data point for each trial in ***Figure 8—figure supplement 1***). To further explore sources of variability in these experiments, using LC16 activation induced backward walking as an example, we reanalyzed the data by pooling results for either all flies of the same trial (per trial) or all trials of the same fly (per fly). This revealed different degrees of variability both across flies within the same trial and across trials for the same fly. Nonetheless, this variability does not change our conclusion that LC16 activation results in a strong backward walking response.

DOI: 10.7554/eLife.21022.022

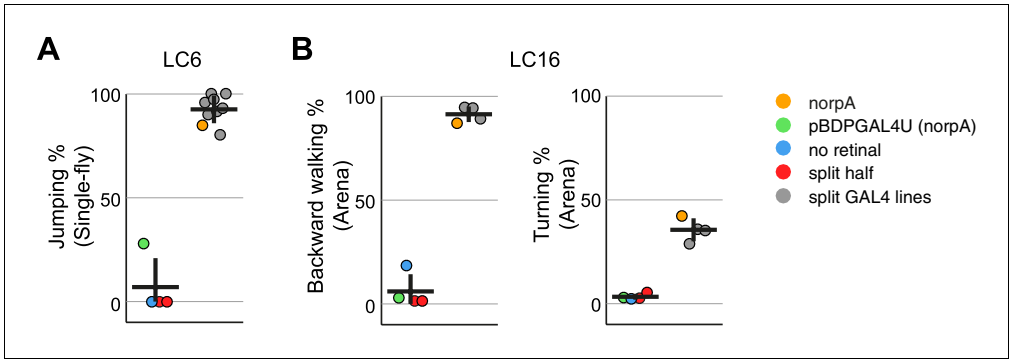

Figure 9. Experiments with additional LC6 and LC16 driver lines confirm the activation phenotypes of these cell types. (**A**,**B**) Behavioral penetrance for different controls and multiple split-GAL4 driver lines for (**A**) jumping (flies that jumped within 200 ms of stimulation onset) with LC6 controls based on the OL0077B driver line and (**B**) backward walking and turning with LC16 controls based on the OL0046B driver line. Each dot represents an experiment done with a different genotype: orange, LC neuron activation in blind norpA flies that also carry an LC6 (**A**) or LC16 (**B**) split-GAL4 line; green, pBDPGAL4U control in blind norpA flies; blue, flies reared on food without supplemental retinal; red, split-GAL4 DBD or AD halves; grey, genetically distinct split-GAL4 driver lines with targeted expression in LC6 (**A**) or LC16 (**B**). Horizontal and vertical lines indicate mean and standard deviation, respectively, for the control group and split-GAL4 group. The genotypes of the driver lines, behavioral penetrance and total trial and fly counts are listed in ***Supplementary file 1B***. Expression patterns of the split-GAL4 driver lines used are shown in ***Figure 9—figure supplement 1***.

DOI: 10.7554/eLife.21022.023

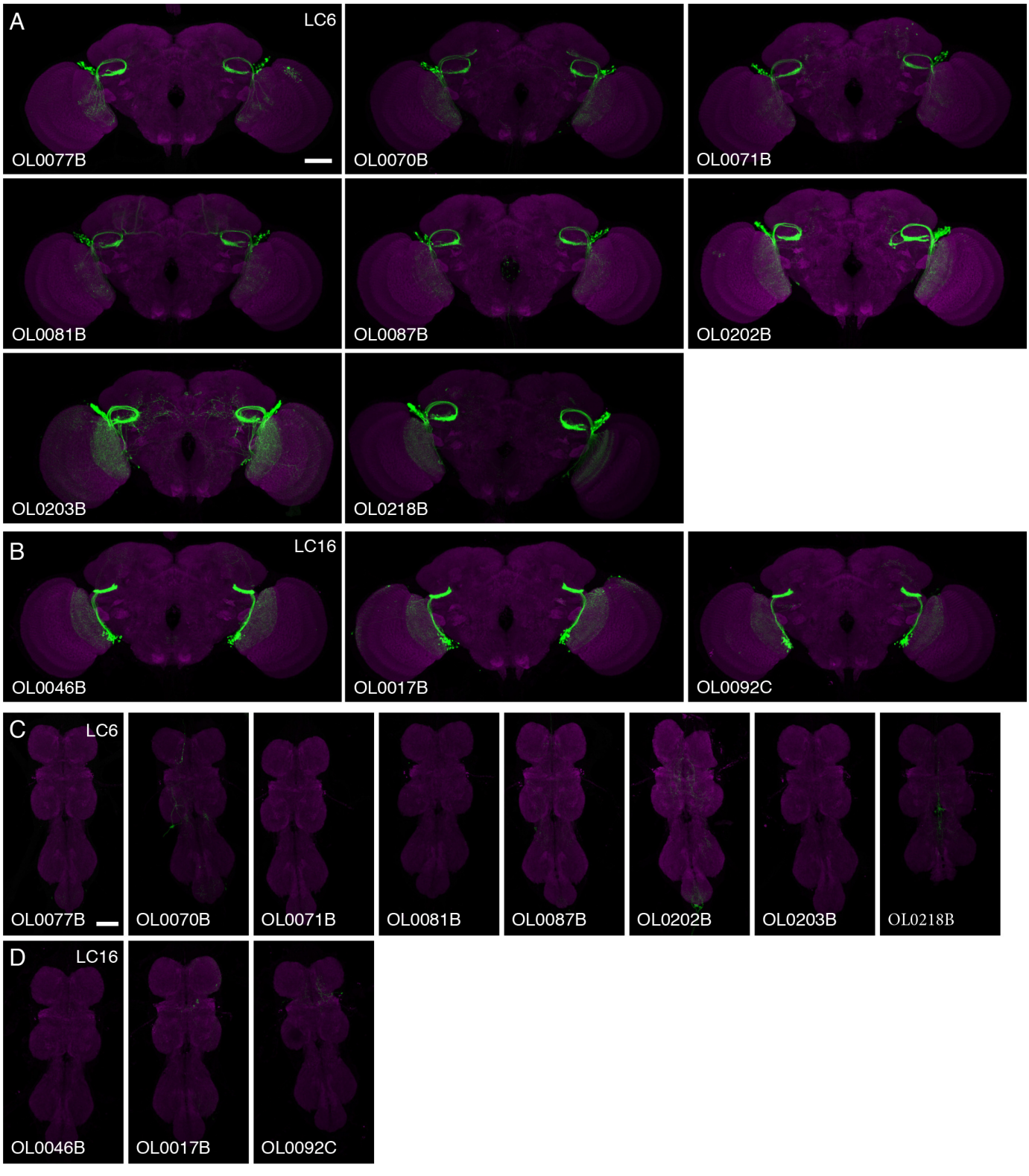

Figure 9—figure supplement 1. Expression patterns of multiple split-GAL4 driver lines for LC6 and LC16. Brain (**A,B**) and VNC (**C,D**) expression patterns of split-GAL4 drivers for LC6 (**A,C**) and LC16 (**B,D**). Split-GAL4 driven expression of 20xUAS-CsChrimson-mVenus (insertion in *attP18*; visualized using anti-GFP antibody labeling; green) and a neuropil marker (anti-Brp, magenta) are shown. Imaging parameters and brightness or contrast

Figure 9—figure supplement 1 continued on next page

Figure 9—figure supplement 1 continued

adjustments were identical within each brain/VNC pair but not across all images. OL0077B and OL0046B images are the same as those shown in ***Figure 2*** and ***Figure 2—figure supplement 1***. Scale bar represents 50 μm. Original confocal stacks are available from www.janelia.org/split-GAL4.
DOI: 10.7554/eLife.21022.024

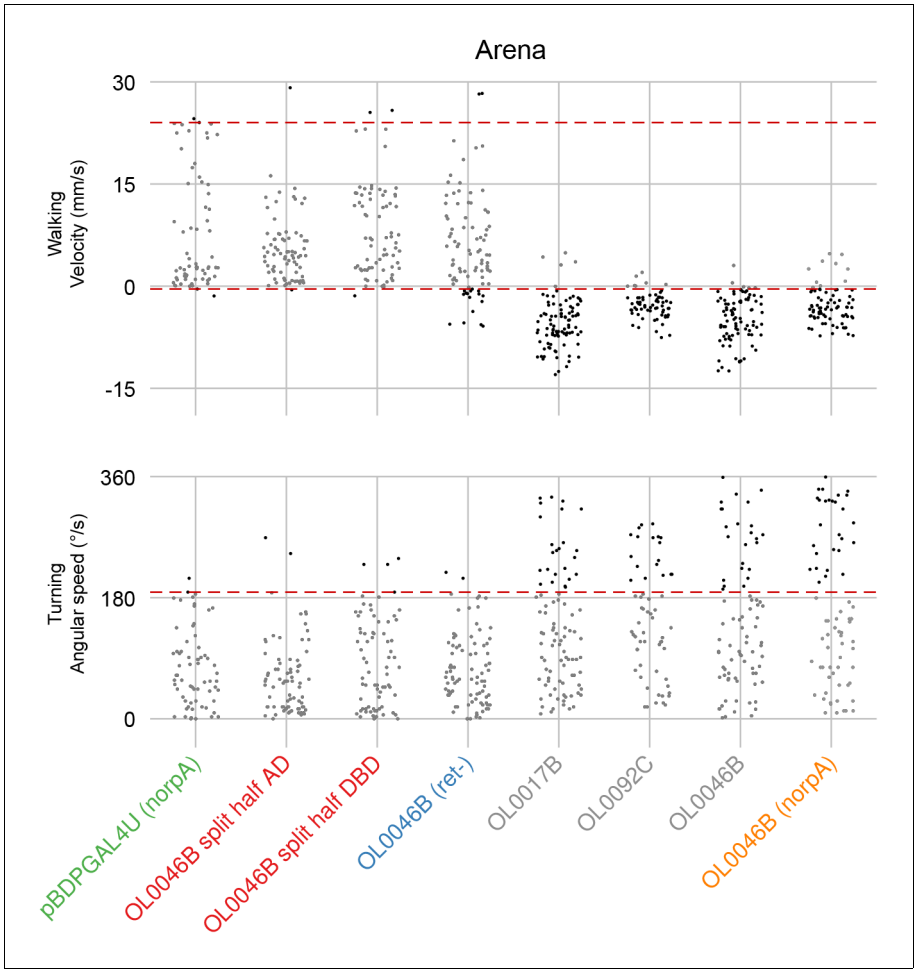

Figure 9—figure supplement 2. Quantification of LC16 activation induced locomotor behaviors and determination of behavioral penetrance. Jitter plots show the distribution of mean velocity and angular speed during optogenetic stimulation of multiple LC16 split-GAL4 driver lines and control lines. Color codes are the same as in ***Figure 9***. Penetrance was determined as in ***Figure 8—figure supplement 1E***.
DOI: 10.7554/eLife.21022.025

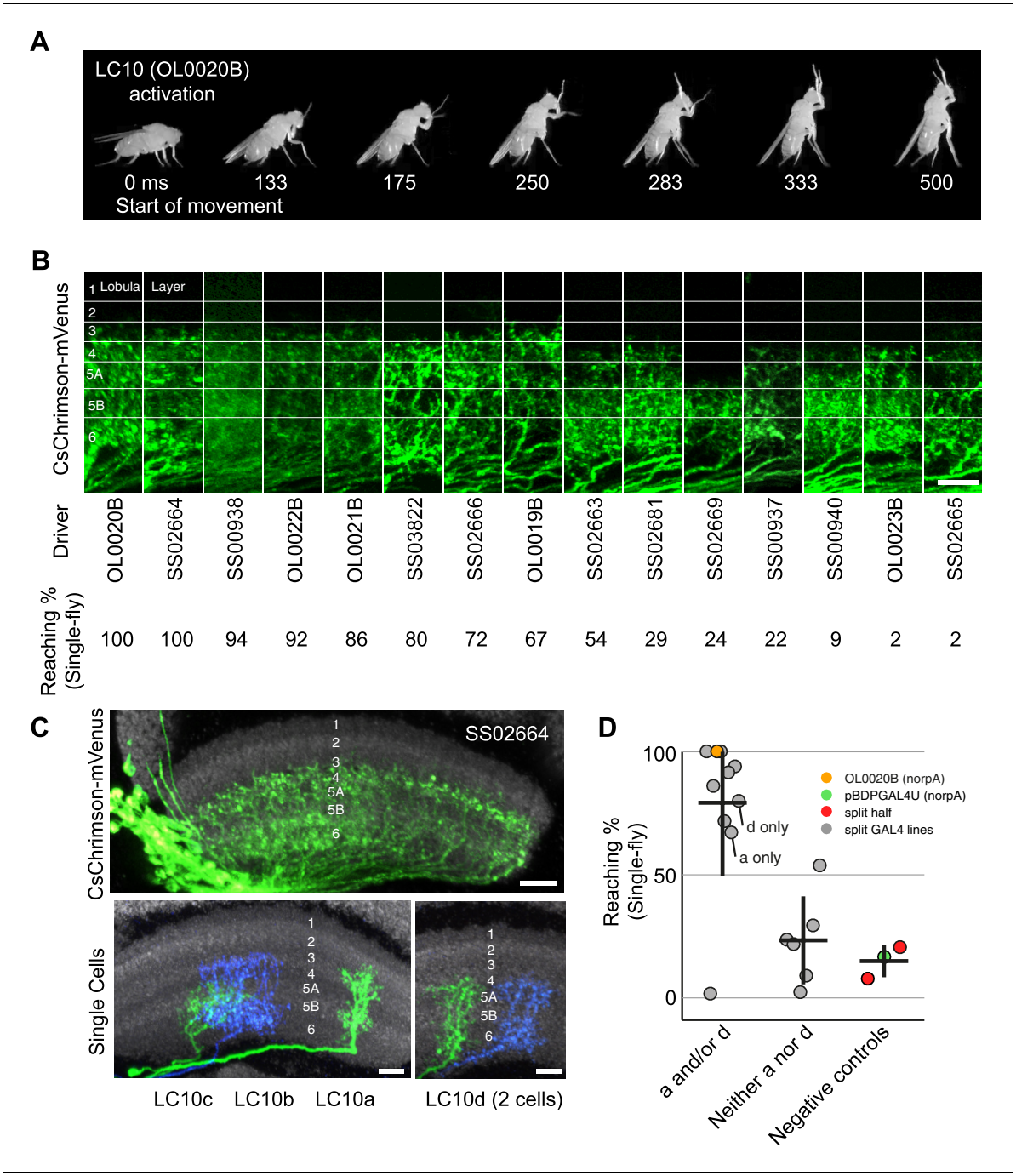

Figure 10. Reaching behavior resulting from activation of LC10 subtypes. (**A**) Representative video images of a fly exhibiting reaching behavior in the single-fly assay. Time stamps indicate milliseconds (ms) after the start of reaching. (**B**) Comparison of lobula layer patterns and penetrance of reaching upon optogenetic activation for 15 LC10 split-GAL4 lines. The images show reconstructed views of CsChrimson expression in the lobula (generated using Vaa3D and manually aligned using the anti-Brp reference marker). Approximate layer positions are indicated on the left. Scale bar represents 10 µm. CsChrimson expression using two additional LC10 driver lines (SS00941 and SS00942) resulted in unexpected uncoordinated behaviors in response to optogenetic activation that precluded analyses of reaching behavior. These lines, which are related as they only differ from each other in the insertion site of the AD hemidriver (see ***Supplementary file 1B***), were therefore excluded from further analyses. (**C**) Single cell labeling reveals subtype expression patterns of LC10 driver lines. Overall lobula expression of an LC10 split-GAL4 line (SS02664) (top panel; displayed as in **B**) and examples of MCFO labeled single cells from this line (bottom panels) are shown. LC10 subtypes (indicated below the images) of single cells were assigned based on layer pattern, arbor size and shape as follows: LC10c cells mainly arborize in layer Lo5B with some processes in the adjacent layers. LC10a cells also have arbors in Lo5B, but differ from LC10c by having additional processes in the more distal layers Lo2, Lo3 and Lo4. LC10b and LC10d differ from LC10a and LC10c by having major arbors in Lo6 and only few processes in Lo5B. Their distal arbors reach Lo4. LC10b cells are wider than LC10d cells

Figure 10 continued on next page

Figure 10 continued

and show many small varicosities (presumably presynaptic sites; compare ***Figure 5—figure supplement 2E***) in Lo6. LC10 neurons also differ in their axonal paths in the AOTu: LC10a and LC10d axons run both dorsally and ventrally, and LC10b and LC10c only ventrally (***Figure 3G***; also see ***Figure 10—figure supplement 1***). Scale bars represent 10 μm. (**D**) Reaching penetrance observed upon activation of the LC10 split-GAL4 drivers and various control lines in the single-fly assay. Split-GAL4 drivers are grouped by expression patterns in the LC10 subtypes: either subtype a and/or d, or neither a nor d. Driver lines were included in the 'a and/or d' category if two or more cells of these types were identified in MCFO experiments (see ***Figure 10—figure supplement 2***). Colors representing various controls and split-GAL4 driver lines are the same as those in ***Figure 9***.

DOI: 10.7554/eLife.21022.026

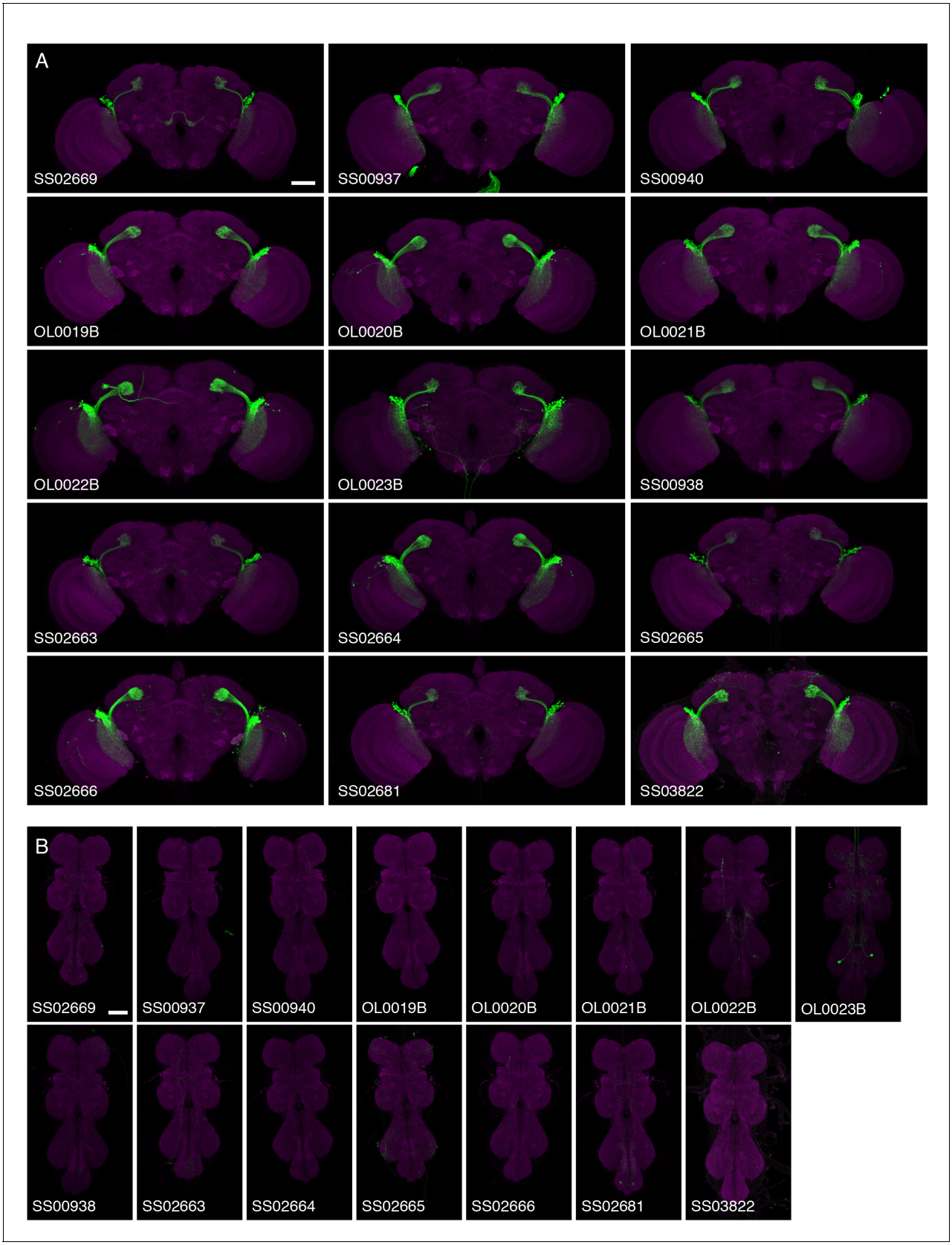

Figure 10—figure supplement 1. Expression patterns of LC10 split-GAL4 driver lines. Brain (**A**) and VNC (**B**) expression patterns using 20xUAS-CsChrimson-mVenus in *attP18* visualized with an anti-GFP antibody (green) and a neuropil marker (anti-Brp, magenta) are shown. While some driver

Figure 10—figure supplement 1 continued on next page

Figure 10—figure supplement 1 continued

lines also had expression in a few non-LC10 cells, none of these additional neurons was consistently present in lines with the reaching behavior. Imaging parameters and brightness or contrast adjustments were identical for each brain/VNC pair but not across all images. OL0020B and OL0023B images are the same as those shown in ***Figure 2*** and ***Figure 2—figure supplement 1***. Scale bar represents 50 μm. Original confocal stacks are available from www.janelia.org/split-GAL4.

DOI: 10.7554/eLife.21022.027

A

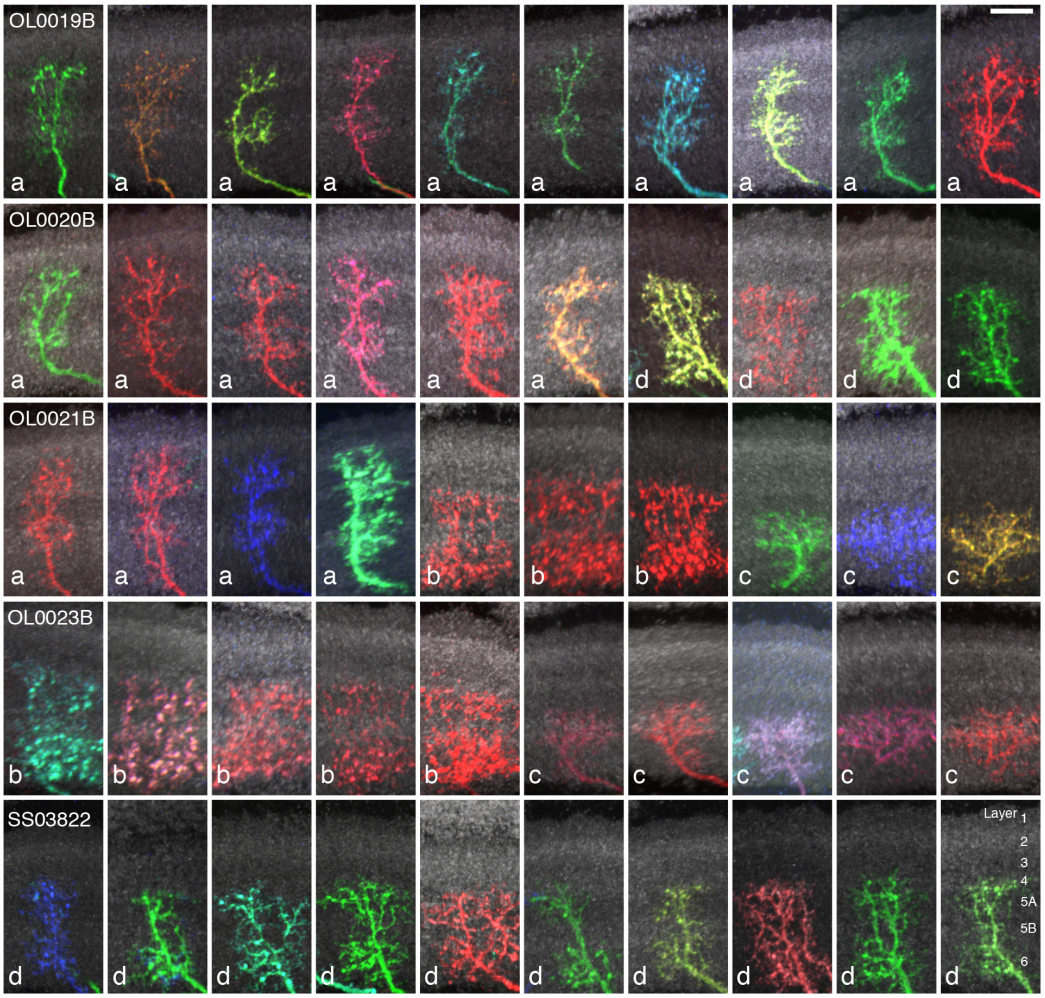

B

Line	Flies	Total cells	LC10a	LC10b	LC10c	LC10d	Summary
OL0019B	10	120	120	0	0	0	a
OL0020B	5	81	44	0	0	37	a,d
OL0021B	3	62	26	17	9	0	a,b,c
OL0022B	5	49	30	0	0	19	a,d
OL0023B	8	77	0	42	35	0	b,c
SS00937	4	38	0	29	9	0	b,c
SS00938	6	47	5	24	8	10	a,b,c,d
SS00940	6	68	1	21	46	0	(a),b,c
SS02663	14	128	0	59	69	0	b,c
SS02664	8	24	9	4	5	6	a,b,c,d
SS02665	7	13	0	4	6	3	b,c,d
SS02666	4	18	9	1	1	7	a,(b),(c),d
SS02669	4	8	0	2	6	0	b,c
SS02681	6	14	0	9	5	0	b,c
SS03822	7	52	0	0	0	52	d

Figure 10—figure supplement 2. Stochastic single cell labeling reveals LC10 subtype expression patterns of the LC10 split-GAL4 driver lines. (**A**) Examples (10 per driver line) of MCFO-labeled LC10 cells from five different lines. Subtype classification is indicated for each cell (white lowercase

Figure 10—figure supplement 2 continued on next page

Figure 10—figure supplement 2 continued

letters). Anti-Brp pattern (used to facilitate comparison of layer positions across specimens) is shown in grey; views were generated using Vaa3D. Layer patterns of these projection images were manually aligned using the anti-Brp marker. To do so, the scale of some images was slightly adjusted to compensate for the non-uniform depth of the lobula. Approximate layer positions are indicated in the bottom right panel. Scale bar represents 10 μm. (**B**) Summary of LC10 MCFO results. For each driver line, the number of MCFO-labeled LC10 cells of each subtype was determined for the indicated number of fly brain samples. Some LC10 cells that were located at an edge of the lobula neuropil or overlapped with other labeled cells and thus could not be identified were excluded from the counts. Total cells refer to the number of all LC10 cells that were assigned a subtype. Subtypes that were only seen as single labeled cell are in parentheses in the summary.

DOI: 10.7554/eLife.21022.028

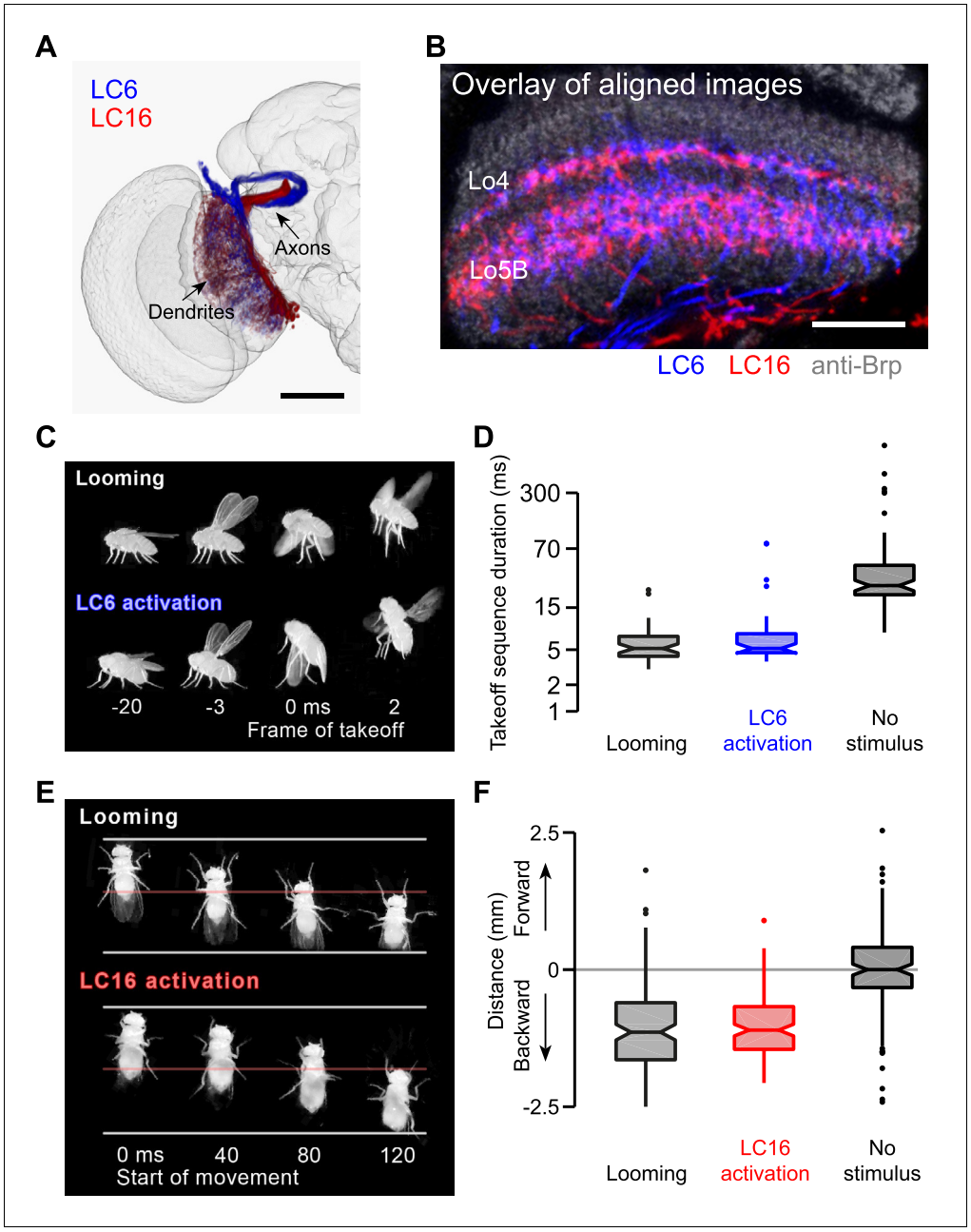

Figure 11. LC6 and LC16 activation behaviors resemble avoidance responses evoked by visual looming. (**A**) LC6 and LC16 project to adjacent, non-overlapping target glomeruli. The image was generated using a 3D image rendering software (FluoRender) (***Wan et al., 2012***) on aligned confocal images. (**B**) LC6 and LC16 have similar layer patterns in the lobula. An overlay of substack projections of aligned image stacks is shown. Anti-Brp reference marker is in grey. (**C**) Representative video images from the single-fly assay showing that a looming stimulus and LC6 activation evoke very similar coordinated behavioral sequences, which include wing elevation, middle leg extension and initiation of flight. Time stamp is set at 0 ms for the frame of takeoff. Negative and positive values are for frames before and after takeoff, respectively. (**D**) Notched box plots showing the duration of the takeoff sequence measured as the time from the first moment of wing movement to the last moment of tarsal contact with the ground after the stimulus (Mann-Whitney test, $p=0.29$ between looming and LC6 activation, and $p<0.001$ between LC6 activation and no stimulus). (**E**) Representative video images from the single-fly assay showing that a looming stimulus and LC16 activation evoke very similar backward walking behaviors. Time stamp is set at 0 ms for the start of backward walking. (**F**) Total distance flies walked on the platform of the single-fly assay. Positive and negative values are for forward and backward walking, respectively (Mann-Whitney test, $p=0.71$

Figure 11 continued on next page

Figure 11 continued

between looming and LC16 activation, and $p<0.001$ between LC16 activation and no stimulus). Scale bars represent 50 μm (**A**) or 20 μm (**B**).

DOI: 10.7554/eLife.21022.029

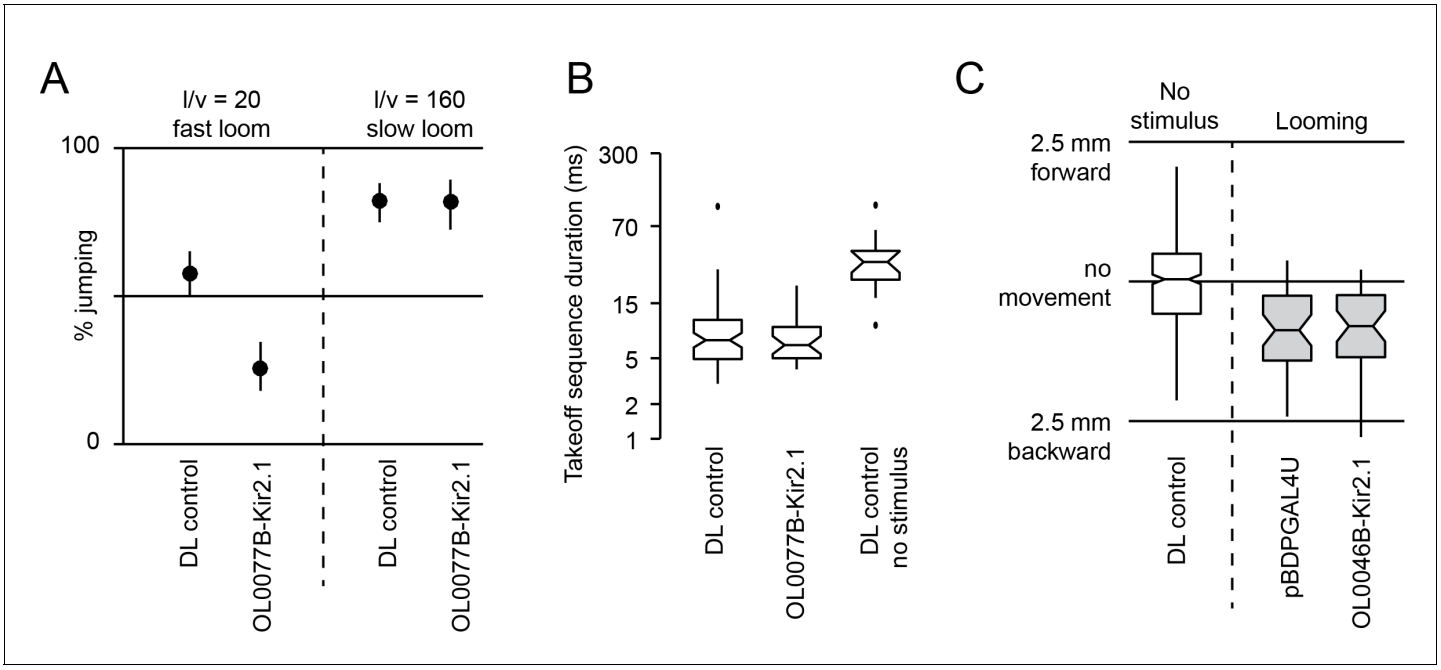

Figure 11—figure supplement 1. Behavioral consequences of silencing LC6 and LC16 by Kir2.1 expression. Split-GAL4 driver lines OL0077B (LC6, **A–B**) or OL0046B (LC16, **C**) were crossed to flies with pJFRC49-10XUAS-IVS-eGFPKir2.1 in a DL strain background. pBDPGAL4U crossed to the same effector or DL flies were used as controls. (**A,B**) Looming stimuli were presented at an elevation of 45˚, an azimuth of 90˚, and an l/v of 20 (as in ***Figure 11C,D***). In addition, a slow stimulus (using an l/v of 160) was included in (**A**) since calcium imaging suggests LC6 is tuned to slower looms (***Figure 12—figure supplement 1***). Confidence intervals were determined using the Clopper-Pearson method. Fly counts for each experiment from left to right are 170, 117, 141, and 89. (**B**) Notched box plots showing the duration of the takeoff sequence (as in ***Figure 11C***). (**C**) Looming stimuli were presented as in ***Figure 11E–F***, specifically chosen to induce backward walking. Total distance flies walked on the platform of the single-fly assay is shown. Fly counts from left to right are 396, 43, and 40.

DOI: 10.7554/eLife.21022.030

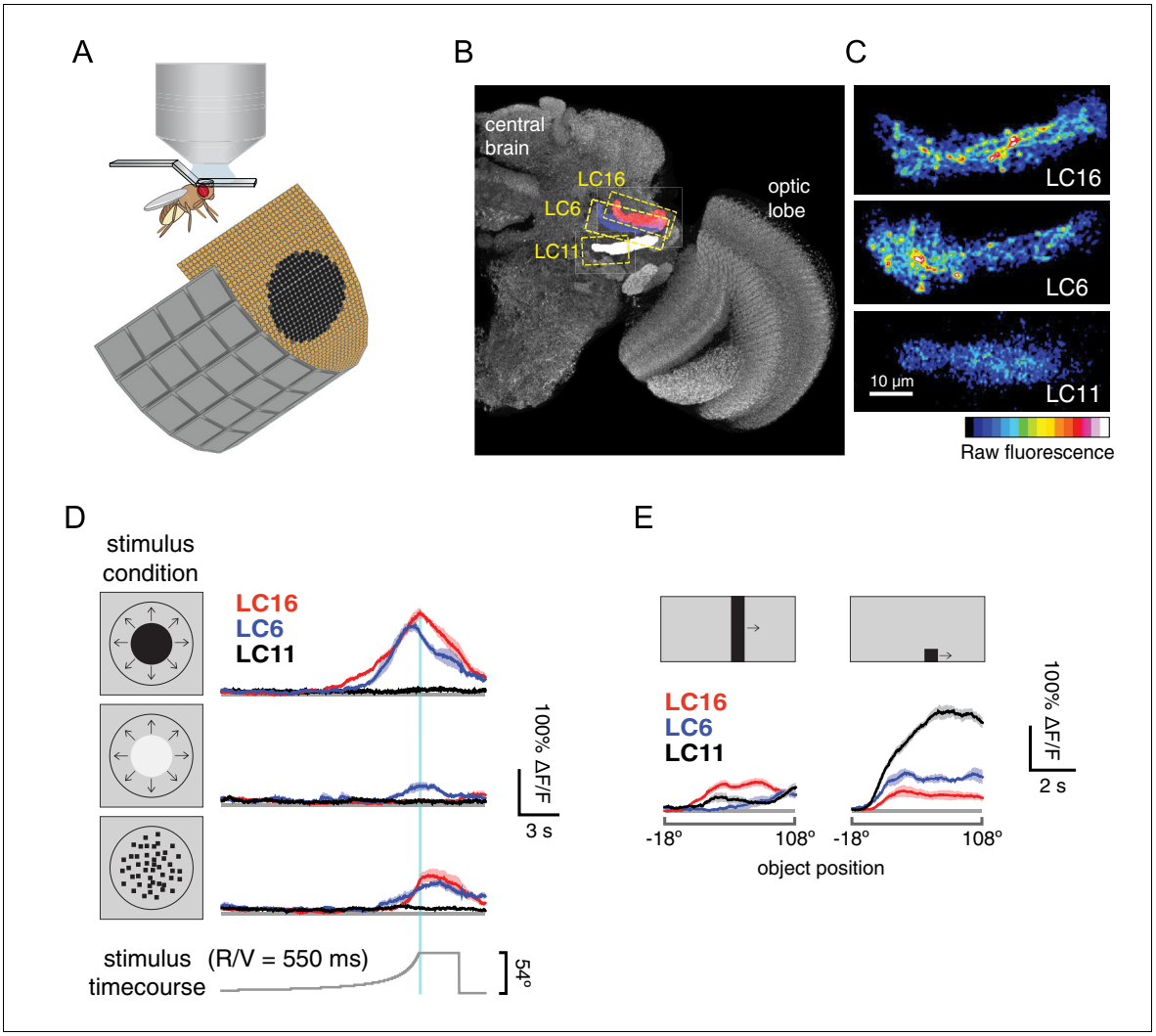

Figure 12. LC16 and LC6, but not LC11, respond to visual looming stimuli with robust calcium increases. (**A**) Visual stimuli evoked calcium responses of LC neurons were imaged in head-fixed flies. (**B**) The axon terminals of LC cells bundle to form cell-type specific glomeruli (subset shown in **C**). We imaged from a single glomerulus by using spilt-GAL4 lines labeling individual cell-types (LC16, LC6 or LC11). Representative regions for calcium imaging experiments are marked with the yellow dashed rectangles. Exemplary responses of LC16, LC6 and LC11 to a slow dark looming disk are shown (**C**; each single frame taken from the peak response of an individual fly, distinct genotypes were used to image from each glomerulus). (**D**) LC16, LC6 and LC11 responses to looming visual stimuli are shown for three variants of the stimulus (from top to bottom: dark looming disk, bright looming disk, luminance-matched) expanding at r/v = 550 ms (n = 5 per genotype). Error bars indicate mean ± SEM. Statistics were performed on mean ΔF/F during a time window in which the response peaks (2 s before and after the looming stimulus stops expanding). (**E**) As a comparison to looming stimuli, we also presented moving object stimuli that contain local motion that is distinct from looming. LC11 responds strongly to the motion of the small (9°x9°) spot, but not the long bar (9°x72°) moving object. The objects moved at 22.5°/s, starting 18° left of the visual midline and stopping 108° to the right of the midline. Statistics were performed on mean ΔF/F during the whole stimulus epoch.

DOI: 10.7554/eLife.21022.031

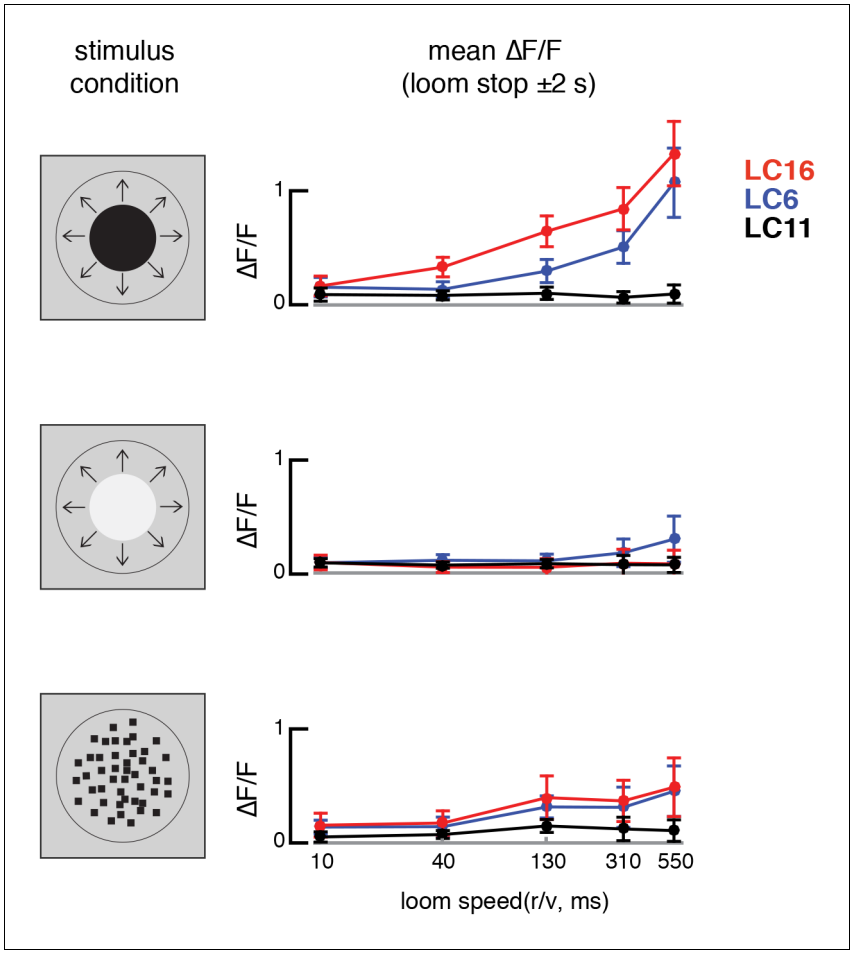

Figure 12—figure supplement 1. LC16 and LC6 are tuned to slower looming speeds. Stimulus evoked calcium responses to different loom speeds. The responses are mean ΔF/F during a time window in which the response peaks (2 s before and after the looming stimulus stops expanding). Stimuli from top to bottom rows: dark looming disk, bright looming disk, luminance-matched.

DOI: 10.7554/eLife.21022.032

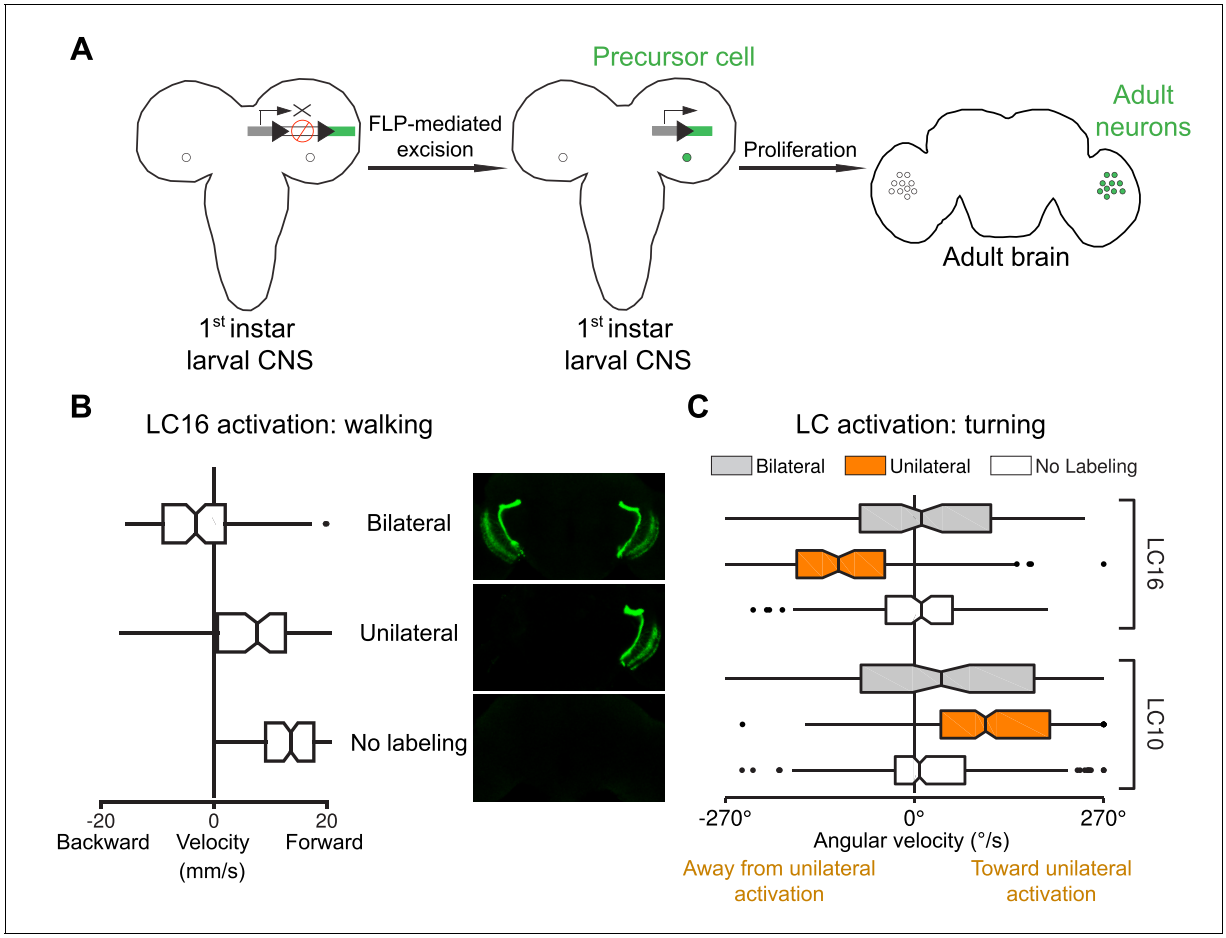

Figure 13. Behavioral responses to unilateral LC neuron stimulation differ from bilateral activation behaviors and are directional. (**A**) Schematic illustration of a genetic method for stochastic labeling and activation of LC neurons. A 'stop-cassette' reporter (pJFRC300-20XUAS-FRT>-dSTOP-FRT>-CsChrimson-mVenus in *attP18*) was used for Flp-recombinase mediated control of CsChrimson expression. This reporter/effector construct (small schematic in the right brain hemisphere of the larval brains in the illustration) is based on the 'Flp-out' design (***Struhl and Basler, 1993***). It contains 20 Upstream Activating Sequences (UAS) and a core promoter (grey rectangle) for GAL4-activated expression, a transcriptional terminator (white rectangle with a red prohibition sign) flanked by Flp-recombinase target (FRT) sites (black triangles), and a CsChrimson-mVenus fusion gene (green rectangle). Heat shock induces expression of the Flp-recombinase which can excise the transcriptional terminator, allowing expression of CsChrimson-mVenus under the control of a split-GAL4 driver (not shown). By expressing a limiting amount of Flp-recombinase early in development (first instar larval stage), stochastic stop-cassette excision occurs in LC precursor cells, generating adults in which most or all neurons of one LC neuron type (determined by the split-GAL4 driver) express CsChrimson-mVenus in either no, one, or two optic lobes. (**B**) Strong backward walking behavior requires bilateral LC16 activation. Notched box plots showing the distribution of mean velocity for bilateral LC16 activation (trial count = 101, fly count = 10), unilateral LC16 activation (trial count = 75, fly count = 7) and no labeling controls (trial count = 114, fly count = 11). Behavioral responses of individual flies were assayed and their brains were subsequently dissected to determine expression patterns. Unilateral LC16 activation produced far less backward walking than bilateral activation (Mann-Whitney test, $p<0.001$). (**C**) Unilateral activation of LC16 and LC10 induces aversive and attractive turning, respectively. Notched box plots showing the distribution of mean angular velocity for different labeling categories of LC16 and LC10: For LC16, trial and fly counts are the same as in (**B**). For LC10, bilateral (trial count = 91, fly count = 8), unilateral (trial count = 268, fly count = 24) and no labeling (trial count = 281, fly count = 22). For unilateral activation, behavioral data from animals with labeling only on the left brain hemisphere were reversed and combined with those from animals with labeling only on the right brain hemisphere. In addition to flies with clear bilateral or unilateral expression, 18 flies in the LC10 stochastic activation experiments had expression in both brain halves but showed differences in the apparent number of labeled LC10 cells between the hemispheres. Because of the wide range of these labeling differences we did not include these flies in the above analysis. However, the behavioral results for this group also showed a turning bias towards the side with stronger labeling (see ***Figure 13—figure supplement 1***), suggesting that even small differences of LC10 activation between the two hemispheres may be sufficient to induce ipsilateral turning.

DOI: 10.7554/eLife.21022.033

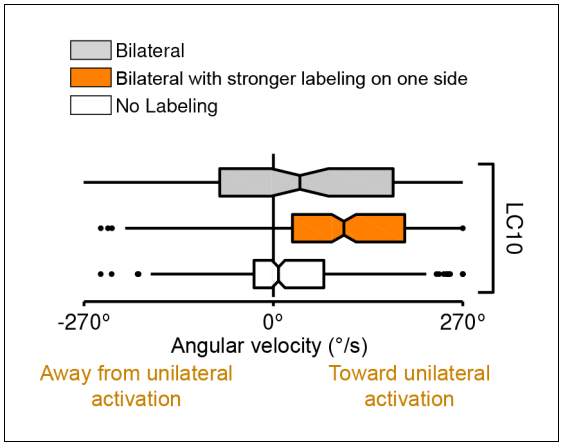

Figure 13—figure supplement 1. Turning behavior of LC10 flies with bilateral labeling that is stronger in one brain hemisphere (trial count = 212, fly count = 18). Data for flies with uniform bilateral expression or no labeling are the same as in the main Figure and included for comparison.
DOI: 10.7554/eLife.21022.034